RC 20398 (3/25/96)
Physical Sciences

IBM Research Report

BAND STRUCTURE, DEFORMATION POTENTIALS, AND CARRIER MOBILITY IN STRAINED Si, Ge, AND SiGe ALLOYS

M. V. Fischetti and S. E. Laux

IBM Research Division
T.J. Watson Research Center
Yorktown Heights, New York

IBM Research Division
Almaden · T.J. Watson · Tokyo · Zurich

BAND STRUCTURE, DEFORMATION POTENTIALS, AND CARRIER MOBILITY IN STRAINED Si, Ge, AND SiGe ALLOYS

M. V. Fischetti and S. E. Laux

IBM Research Division, Thomas J. Watson Research Center
P. O. Box 218, Yorktown Heights, NY 10598

Using nonlocal empirical pseudopotentials, we compute the band structure and shear deformation potentials of strained Si, Ge, and SiGe alloys. Fitting the theoretical results to experimental data on the phonon-limited carrier mobilities in bulk Si and Ge, the dilatation deformation potential Ξ_d is found to be 1.1 eV for the Si Δ-minima, -4.4 eV for the Ge L-minima, corresponding to a value for the valence band dilatation deformation potential a of approximately 2 eV for both Si and Ge. The optical deformation potential d_0 is found to be 41.45 and 41.75 eV for Si and Ge, respectively. Carrier mobilities in strained Si and Ge are then evaluated. The results show a large enhancement of the hole mobility for both tensile and compressive strain along the [001] direction, but only a modest enhancement (approximately 60%) of the electron mobility for tensile biaxial strain in Si. Finally, from a fit to carrier mobilities in relaxed SiGe alloys, the effective alloy scattering potential is determined to be about 0.5 eV for electrons, 0.9 ± 0.1 eV for holes, and the low-field mobilities in strained alloys can be evaluated. The results show that alloy scattering completely cancels any gain expected from the lifting of the valleys/bands degeneracy caused by the strain.

PACs: 71.22.+i 71.70.Fk 72.20.Fr

I. INTRODUCTION AND SYNOPSIS

The calculations of the band structure and of the carrier mobilities in strained Si and SiGe alloys have so far been decoupled. On the one hand, band structure calculations based on self-consistent[1] or empirical[2–4] pseudopotentials, coupled to a 'model-solid approach'[5], on the coherent potential approximation[6], or on the tight-binding approximation[7–9], have provided important information concerning energy shifts at symmetry points, deformation potentials, band offsets at heterointerfaces, and properties of superlattices. However, the determination of other transport parameters, such as effective masses and accurate (within tens of meV) energy splittings at symmetry points, has either been left unexplored, or has produced results of inadequate accuracy for transport calculations[7]. Notable exceptions are Refs. 2 and 4, where effective masses have been carefully studied, and Ref. 6 which is, to our knowledge, the only example, albeit a partial one, of band-structure results applied to the calculation of the electron mobility. On the other hand, and for these reasons, mobility calculations, even of remarkable sophistication, have relied on scattered and inconsistent data on band-structure and deformation potential parameters, such as the $\mathbf{k}\cdot\mathbf{p}$ approaches of Refs. 10–15, or had to depend on simplified band-structure and scattering models[16–21].

In this paper we unify band-structure and mobility calculations, and obtain a consistent picture in satisfactory agreement with available experimental information. In this way we minimize the number of empirical parameters needed to 'fit' the mobility in known cases, and, hopefully, bolster our confidence in the results concerning cases yet to be explored experimentally.

The paper is organized as follows: In Sec. II, after a brief discussion of the crystal structure under strain, we move to band structure calculations. Nonlocal empirical pseudopotentials with spin-orbit interaction[22] are used, because they have been shown to be sufficiently accurate, while at the same time allowing some flexibility to tailor important results (mainly, effective masses[4] and energy splittings of bands or valleys near the band extrema) which are crucial in the determination of the carrier mobility. Results from pseudopotential calculations are also used to extract valence band $\mathbf{k}\cdot\mathbf{p}$ parameters, needed to facilitate the numerical evaluation of the hole mobility, and the uniaxial deformation potentials which control the strength of the carrier-phonon interaction.

In Sec. III we revisit the problem of calculating mobilities in bulk, unstrained Si and Ge, in order to determine the few parameters needed to calculate low-field mobilities in strained materials: In addition to electron intervalley scattering parameters, which we take from the 'proven' Monte Carlo literature (but see below for a discussion on why the word 'proven' must be taken with a grain of salt), we still need information about the dilatation deformation potentials Ξ_d and a, the hole/optical-phonon deformation potential, d_0, and, for alloys, the alloy scattering potentials, ΔU. Remarkably, the electron and hole mobilities are strictly coupled, since they are strongly controlled by the dilatation deformation potentials Ξ_d and a, respectively. These, in turn, are linearly related, thanks to the band-structure calculations in strained Si and Ge which provide the value of $\Xi_d - a$. A fit to the electron mobility at 300 K in bulk Si and Ge leaves no room for uncertainties, only one value of a (therefore, of Ξ_d) being consistent with the measured electron *and* hole mobilities. The major source of errors will turn out to be the scatter of the experimental mobility data. The value of the optical deformation potential d_0 can finally be determined, with the major errors once more arising from experimental uncertainties. The determination of all transport parameters, in particular the poorly known and hard-to-measure dilatation deformation potentials, should be regarded as a major by-product of our work.

In Sec. IV we finally move to the calculation of mobilities in strained materials. For the well studied case of electrons in strained Si (see, for example, Refs. 20 and 23–31), we confirm the mobility enhancement under biaxial tensile strain, but we are forced to leave unanswered many questions about the quantitative amount of the effect. For the less frequently investigated case of holes[13,14,32], the mobility enhancement is even more pronounced and qualitatively independent of strain type, compressive or tensile. We also discuss carrier mobilities in strained Ge, problem of quite academic interest, and therefore largely unexplored. Finally, before moving to strained $Si_{1-x}Ge_x$ alloys, we must determine the effective alloy scattering potentials for the conduction and valence bands. We do so by fitting the room-temperature electron and hole mobilities in bulk, unstrained Si and Ge and the experimental 300 K mobilities in relaxed $Si_{1-x}Ge_x$ alloys at various Ge mole fractions. Unfortunately, here we have to rely on rather old experimental data. The importance of alloy scattering will be found to be overwhelming, so much as to negate all positive effects resulting from the strain in SiGe alloys for all but the highest strain.

II. BAND STRUCTURE AND UNIAXIAL DEFORMATION POTENTIALS

A. Crystal Structure

In this brief section we set the notation and recall elementary concepts related to the crystal structure of strained materials. As a rule, we shall identify by square brackets, $[lmn]$, crystal directions identified by their Miller indices, l, m, and n, by bra-kets, $<lmn>$, the directions of crystallographic planes, once again identified by Miller indices. For cubic crystals, the $[lmn]$ direction is thus normal to the $<lmn>$ plane. Furthermore, we shall take the z-axis along the [001] direction. Uniaxial strain along the [001] direction is related, as discussed below, to biaxial strain (usually of opposite sign, for a negative Poisson ratio) in the <001> plane. The direction along the z-axis will be referred to as to the direction 'normal to the layer', or 'out-of-plane', while directions lying on the (x, y)-plane (*i. e.*, the <001> plane) will be referred to as directions on the 'plane of the layer', or, for short, 'in-plane'.

In handling the structure of strained Si, Ge, and SiGe alloys we have followed Van de Walle and Martin[1]. In particular, we denote by $a_{||}$ the lattice constant of the substrate material (*i. e.*, the in-plane lattice constant of the strained layer). The in-plane component, $e_{||}$, of the strain tensor is simply $a_{||}/a_0 - 1$, where a_0 is the lattice constant of the relaxed layer material. In the linear (small strain) approximation, the component of the strain tensor in the direction normal to the interfaces of the layer, $e_{\perp}$, is related to the in-plane strain via $e_{\perp} = -De_{||}$, where D is given in Ref. 1 (see Eqns. (4a)-(4c) of this reference) as a function of the crystal orientation and of the elastic constants, c_{11}, c_{12}, and c_{44}. For <001> surfaces on the (x, y)-plane, the strain tensor is diagonal with $e_{\perp} = e_{zz}$ and $e_{||} = e_{xx} = e_{yy}$, while for [111] strain (normal to <111> surfaces), the strain tensor has only two independent components, all diagonal terms being equal to e_{xx} and all off-diagonal terms being equal to e_{xy}, with $e_{xx} = (e_{\perp} + 2e_{||})/3$ and[33] $e_{xy} = 2(e_{\perp} - e_{||})/3$.

For the lattice constant, $a_{SiGe}(x)$, of relaxed $Si_{1-x}Ge_x$ alloys we have used the experimental results by Logan *et al.*[34], approximated analytically as:

$$a_{SiGe}(x) = a_{Si}(1-x) + a_{Ge}x - bx(1-x), \tag{1}$$

with a parameter $b = 1.88 \times 10^{-3}$ nm, yielding 0.34 % of maximum bowing at a mole fraction x of 0.5.

In addition to the 'stretching' of the unit cell caused by the strain, in computing the band structure of Si and Ge under strain in the [111] direction we have also accounted for an additional displacement, $\mathbf{u}$, of the ions in the unit cell, as described by Van De Walle and Martin[1], $\mathbf{u} = -(\zeta/6)a_0(e_{\perp} - e_{||})(\hat{\mathbf{x}} + \hat{\mathbf{y}} + \hat{\mathbf{z}})$, where $\hat{\mathbf{x}}$, $\hat{\mathbf{y}}$, and $\hat{\mathbf{z}}$ are the unit vectors along the Cartesian axes and the parameter ζ has been obtained theoretically[35].

We list in Table I the values of the material parameters we have employed, obtained either from the compilation in Ref. 36 (for lattice and elastic constants, sound velocities, and phonon energies) or from the aforementioned work by Nielsen and Martin[35]. The valence-band parameters L, M, and N have been derived from $\mathbf{k} \cdot \mathbf{p}$ fits to our results from band-structure calculations.

B. Nonolocal pseudopotentials

The band structures of strained Si, Ge, and SiGe alloys can be obtained from the form factors and spin-orbit parameters reported by Chelikowsky and Cohen[22]. The particular case of strained SiGe alloys has been investigated by Gell[2], mainly focusing on the valence band effective masses, and, more recently, in a systematic study by Rieger and Vogl[4]. In most cases, the main motivation of the study was the band structure *per se*, possibly with emphasis on the band-gap variations with strain and/or alloy composition. On the contrary, our final goal here is the evaluation of the carrier mobility. Therefore, for this and the other reasons stated below, we have taken the following exceptions from the published set of parameters[4,22]:

1. We have used about 100-120 plane waves, fixed by the cutoff energy $E_{cut} = 8$ Ry, without any further approximation.

2. We have included the spin-orbit interaction also in the case of Si. Indeed, a spin-orbit splitting of about 44 meV for the valence bands at the symmetry point Γ is important for the calculation of the hole mobility.

3. We have modified slightly the symmetric form factors $V_s(q)$ at $q = \sqrt{3}(2\pi/a_0)$ for both Si and Ge. For Si, the form factor we have used results in an indirect Γ_{8v}-Δ_{6c} gap of about 1.17 eV, up from the value 1.03 eV we obtain using the parameters of Ref. 22. For Ge, we now obtain energy separations of the minima of the first conduction band at the symmetry points Γ, L, and along the symmetry line Δ, ($E^{(\Gamma)} - E^{(L)} \simeq 138$ meV, $E^{(\Delta)} - E^{(L)} \simeq 185$ meV), which match very closely the experimental values, as required for accurate calculation of the electron mobility. We obtain an indirect Γ_{8v}-L_{6c} energy gap of 0.79 eV. In addition, a square nonlocal d-well has been used for Ge, in place of the Gaussian well used in Ref. 22. For this reason the well-depth has been slightly rescaled.

4. Since the calculation of the band structure of strained Si and Ge, and of SiGe alloys requires the knowledge of the local terms of the pseudopotentials also at wavevectors $\mathbf{q}$ others than points $\mathbf{G}$ of the reciprocal (unstrained) lattices, we have obtained the local contribution to the symmetric pseudopotential, $V_s(q)$ for arbitrary values of q by interpolating the values at $q = \sqrt{3}$, $\sqrt{8}$, and $\sqrt{11}(2\pi/a_0)$ with an expression of the form[3]:

$$V_s(q) = \frac{1}{\Omega_a} \frac{a_1(q^2 - a_2)}{\exp[a_3(q^2 - a_4)] + 1} \left[\frac{1}{2} \tanh\left(\frac{a_5 - q^2}{a_6} \right) + \frac{1}{2} \right], \tag{2}$$

where Ω_a is the atomic volume. The values of the interpolation parameters a_1 through a_4 are given in Table II in atomic units: Expressing q and Ω_a in atomic units, $V_s(q)$ will be in Hartree atomic units. Multiplication by 2 yields Rydbergs. The values of $a_5 = 5.0$ a.u. and $a_6 = 0.3$ a.u. for both Si and Ge are from Ref. 3. Equation (2) has been obtained by empirically determining the 'slopes' $\partial V_s(G)/\partial G$ in order to obtain band-gap deformation potentials for strained Si and Ge within the range of the experimental data[37], as done by Fridel, Hybertsen, and Schlüter[3]. Note that at long wavelength we have not required $V(0) = -(3/2)E_{F0}$, where E_{F0} is the free-electron Fermi energy[4], in view of the uncertainty surrounding the correct interpolation[3,38–41]. The short-wavelength cutoff, from Ref. 3, is needed to suppress the contribution from the star of the (4,0,0) $\mathbf{G}$-vectors, ignored in the calibration of the form factors in unstrained Si and Ge.

5. We have interpolated all nonlocal and spin-orbit parameters (see Table II) linearly in the mole-fraction x for $Si_{1-x}Ge_x$ alloys. Reference 40 describes in detail the spin-orbit and nonlocal Hamiltonians we have used.

Finally, Table II lists the pseudopotential, spin-orbit, and numerical parameters we have used.

C. Results of band-structure calculations

In addition to their obvious intrinsic interest, the calculated band structure for strained Si and Ge allows the determination of several deformation potentials which influence the carrier mobility. References 1, 42, and 43 provide all the formulae connecting quantitatively the energy shifts and splittings at symmetry points to the shear (or uniaxial), b, d, and Ξ_u, and dilatation, a and Ξ_d, deformation potentials.

In Figs. 1 through 3 we show the energy shifts at symmetry points obtained from our calculations. The cases of Si and Ge strained along the [001] direction are shown in Fig. 1 (a) and (b), respectively. The strain is indicated by the ratio $a_{\|}/a_0$. The shear deformation potentials ($\Xi_d^{(\Delta)}$, b), and the linear combination $\Xi_d^{(\Delta)} + \Xi_u^{(\Delta)}/3 - a$ derived from these results are shown in Table III, together with those ($\Xi_d^{(L)}$, d, and $\Xi_d^{(L)} + \Xi_u^{(L)}/3 - a$) obtained from analogous calculations of the energy shifts under [111] strain (not shown). As also found in Ref. 3, a complicated dependence of the deformation potentials on the strain conditions has rendered the extraction of meaningful values a hard problem, particularly for strain applied along the [111] direction. The values reported in Table III are representative of small-strain situations and deviations should be expected at large strain. Comparing our results to other theoretical and experimental results reported in the literature (either from the compilation of data in Ref. 36 or from Refs. 1, 4, 7 and 44–55), we see a generally satisfactory agreement. The only exception is the calculated value of the quantity $\Xi_d^{(\Delta)} + \Xi_u^{(\Delta)}/3 - a$ for Ge, which is larger than previous theoretical estimates. This results from our choice for the slopes $\partial V_s(G)/\partial G$. While direct experimental information is missing, our choice results not only in a - at least qualitatively - correct band-gap deformation potential for $Si_{1-x}Ge_x$ alloys pseudomorphic to Si <001>, but also in an electron mobility in the Δ valleys of Ge consistent with experiments, as we shall seee below. The 'absolute' energy scale has been fixed by arbitrarily setting the energy of the valence band maximum to zero and by using a value of 2.1 eV for Si, of 2.0 eV for Ge for the valence-band dilatation deformation potential a. This choice will be justified in the next section.

The lines in Fig. 2 illustrate the calculated energy shifts for the relaxed $Si_{1-x}Ge_x$ alloy. The open symbols are the experimental data by Morar and Batson[56] added to the experimental values for the indirect gap by Weber and Aloso[57]. The solid symbols are the energies in Si and Ge at the indicated symmetry points from the data compiled in Ref. 22. Note the satisfactory agreement with the experimental data, in particular the Δ-to-L crossover of the conduction band minimum at a Ge mole fraction of about 85%. In this figure the absolute energy scale has been set by using the alignments of the valence-band maximum to the Fermi level of Au reported by Tiwari and Frank[58] for Si and Ge and simply interpolating linearly the energy at the Γ point (Γ_{8v}) between pure Si and pure Ge.

The two cases of $Si_{1-x}Ge_x$ alloys grown on <001> Si and on <001> Ge substrates are illustrated in Fig. 3(a) and Fig. 3(b), respectively. The solid symbols are the experimental values for the 77 K gap of $Si_{1-x}Ge_x$ alloys grown on <001> Si substrates measured by Lang *et al.*[59]. In agreement with the theoretical results of Refs. 1 and 43, we underestimate the value of the energy gap, while Rieger and Vogl[4] overestimate it somewhat. Note how for alloys grown on <001> Si substrates the alloy remains 'Si-like' (*i. e.*, with a Γ-Δ indirect gap) even in the case of pure Ge, while for alloys grown on Ge substrates the gap crosses over from a Γ-Δ to an L-Δ gap at roughly the same Ge mole fraction seen for the relaxed alloy in Fig. 2. The zero of the energy scale has been set similarly to what was done in Fig. 2.

Finally, the values of the effective masses at significant symmetry points under the conditions of Figs. 1-3 are shown by the open symbols in Figs. 4-6. They are given in units of the free electron mass, m_0, and are compared to experimental data (solid symbols, from the compilation in Ref. 36), when available. The electron effective masses are simply the 'curvature' band-edge masses obtained from the band structure results. We have obtained these by a simple fit to the dispersion in various directions away from the valley minima. While less elegant than the technique used in Ref. 4, this simpler approach allows us also to estimate nonparabolic effects and avoid the problems of the undefined second derivative of the energy-dependence of the depth of the Si s-well, $A_{l=0}(E)$. For the Δ-valleys, the transverse ($m_t^{(\Delta)}$) and longitudinal ($m_l^{(\Delta)}$) masses in both the [100] and [001] valleys are presented. As discussed by Rieger and Vogl[4], while the equienergy surfaces around the two [001] Δ-minima are well approximated by the 'usual' ellipsoids of revolution, ignoring nonparabolicity for now, those around the four [100] Δ-minima can be approximated by oblate or prolate ellipsoids. This requires the use of two transverse masses: One lying on the (x, y)-plane (labeled $m_{t,\parallel}^{(\Delta)100}$ in Figs. 4(a) and 6(a)), the other in the transverse direction normal to the (x, y)-plane (labeled $m_{t,\perp}^{(\Delta)100}$). For Ge this effect is less pronounced, as it can be seen in Fig. 4(c): The values of $m_{t,\parallel}^{(\Delta)100}$ (circles), $m_{t,\perp}^{(\Delta)100}$ (open triangles), and $m_t^{(\Delta)001}$ (open squares) are almost identical. Similar considerations apply to the L-valleys, which must be characterized by two transverse masses: a mass $m_{t,\parallel}^{(L)}$ along the $[1\overline{1}0]$ direction lying on the (x, y)-plane, and a mass $m_{t,\perp}^{(L)}$ along the $[11\overline{2}]$ direction, normal to both the longitudinal axis and the transverse direction $[1\overline{1}0]$ just considered. Although in the linear scale of Fig. 4(c) we cannot distinguish between the two masses, both shown as open diamonds, such a difference can be noticed in the semilogarithmic scale of Fig. 6(c). Note in Fig. 5(a) that the different choice of pseudopotential parameters made by Rieger and Vogl[4] results in a much smaller longitudinal mass in the L-valley of Si ($\simeq 1.66m_0$) compared to our results ($\simeq 1.94m_0$), while the other values for the effective masses are quite similar.

As far as hole masses are concerned, the large anisotropy and nonparabolicity of the valence bands prevents a simple definition of 'curvature' mass. Instead, we have decided to plot the density-of-states (DOS) effective mass at the thermal energy $E_{th} = (3/2)k_B T$ (where k_B is the Boltzmann constant and T the lattice temperature), $m_{d,\alpha}$, where α runs over the valence bands, defined in such a way that:

$$\frac{m_{d,\alpha}^{3/2} E^{1/2}}{2^{1/2}\pi^2\hbar^3} = \frac{1}{(2\pi)^3}\int_0^{2\pi} d\phi \int_0^{\pi} d\theta \sin\theta \; \overline{k}_\alpha^2(E_{th},\theta,\phi) \left|\frac{\partial E^{(\alpha)}(\theta,\phi)}{\partial k}\right|_{k=\overline{k}}^{-1}, \tag{3}$$

is the density of states in band α (per spin state) at the thermal energy. In the non-degenerate limit considered here, this definition agrees within better than 1% with the more rigorous definition of the density-of-states effective mass obtained by integrating the equation above over the equilibrium distribution function (see, for example, Eq. (5) of Ref. 60). In Eq. (3), $\hbar$ is the reduced Planck constant, $\overline{k}_\alpha^2(E,\theta,\phi)$ is the squared magnitude of the hole k-vector at energy E in band α along the direction (θ,ϕ) in k-space away from the Γ point. We have used the six-band (three bands plus spin) $\mathbf{k}\cdot\mathbf{p}$ approximation of Ref. 61 with the spin-orbit Hamiltonian[62]. The L, M, and N parameters we have employed are taken from Ref. 63, since they fit remarkably well the pseudopotential band structure. Their values, reported in Table I, are within the range of the scattered values found in the literature[11,12,45,49,61,64–66]. From a computational point of view, the use of a $\mathbf{k}\cdot\mathbf{p}$ model facilitates the evaluation of Eq. (3), since, for fixed E, θ, and ϕ, we can use the well-known inversion of the $\mathbf{k}\cdot\mathbf{p}$ Hamiltonian, obtaining an eigenvalue problem for the squared magnitude of the k-vector, k^2. Negative values of k^2 yield the complex band structure in the gap, while positive values provide directly the desired result $\overline{k}^2(E,\theta,\phi)$. This procedure also provides directly the eigenstates needed to evaluate the density of states factor $|\partial E(\theta,\phi)/\partial k|_{k=\overline{k}}$.

The resulting hole effective masses are shown in Figs. 4(b) and (d), 5(b), and 6(b) and (d). Note how in unstrained crystals the $v2$ (heavy-hole) and $v1$ (light hole) bands attempt to repel each other away from the Γ point. This results in a larger heavy-hole mass and a smaller light-hole mass. The difference between the $v2$ and the $v1$ masses decreases, as soon as a small amount of strain removes the $v2/v1$ degeneracy at Γ. The strongly anisotropic shape of the strained equienergy surfaces in the valence bands has been discussed at length from an experimental perspective by Hensel and Feher[65], and by Manku and Nathan[66] from a $\mathbf{k}\cdot\mathbf{p}$ point of view. Therefore, we shall not discuss this issue here. We only show in Fig. 7 the hole band-edge masses for the topmost valence bands for [001]-strained Si, and for $Si_{1-x}Ge_x$ alloys conformal to both <001> Si and Ge substrates. The strong reduction of the effective masses is evident in all cases. Comparison with experimental data is complicated by nonparabolicity effects. Recently, Whall and co-workers[67] and Song *et al.*[68] have extrapolated the cyclotron mass to zero magnetic field. Similarly, Cheng and co-workers[69] have extrapolated the measured mass to low densities. In both cases, the extrapolated masses should represent the band-edge masses. Their results are shown in Fig. 7(b).

III. CARRIER MOBILITY IN UNSTRAINED Si AND Ge AND DILATATION DEFORMATION POTENTIALS

As already noticed above, the knowledge of the band structure (and/or effective masses) and of the uniaxial deformation potential is not sufficient to obtain the carrier mobility. The crucial missing piece of information required is the knowledge of the dilatation deformation potentials, a and Ξ_d, for the valence and conduction bands respectively. Actually, the knowledge of either one is sufficient, thanks to the linear relation, Eq. (15) of Ref. 1, connecting them, together with the variation of the energy gap with strain, obtained from band structure calculations. In this section we shall use the experimentally known electron and hole mobilities in Si and Ge to determine these last unknowns. In so doing we set the framework within which carrier mobilities will be computed for the case of strained materials.

Let's consider carriers distributed in many bands (or valleys) labeled by an index α, under homogeneous and nondegenerate conditions, and at steady state. Let's also define the i-th component of a 'formal' relaxation time, $\tau_i^{(\alpha)}(\mathbf{k})$, implicitly as follows:

$$\frac{1}{\tau_i^{(\alpha)}(\mathbf{k})} = \sum_\beta \int \frac{d\mathbf{k}'}{(2\pi)^3} S(\mathbf{k}'\beta;\mathbf{k}\alpha) \left\{ 1 - \frac{v_i^{(\beta)}(\mathbf{k}')\tau_i^{(\beta)}(\mathbf{k}')}{v_i^{(\alpha)}(\mathbf{k})\tau_i^{(\alpha)}(\mathbf{k})} \right\}, \tag{4}$$

where $\mathbf{k}$ is the particle quasi-momentum (measured from the minimum of each band or valley), $v_i^{(\alpha)}(\mathbf{k})$ is the i-th component of the carrier velocity in band α, and $S(\mathbf{k}'\beta;\mathbf{k}\alpha)$ is the total scattering kernel from the state $\mathbf{k}$ in band/valley α to the state $\mathbf{k}'$ in band or valley β. Multiplying the Boltzmann equation by $v_i^{(\alpha)}(\mathbf{k})\tau_i^{(\alpha)}(\mathbf{k})$, summing over the bands or valleys, and integrating over $\mathbf{k}$, we obtain for the i-th component of the current density, $j_i^{(\alpha)}$, due to carriers in band α:

$$j_i^{(\alpha)} = en^{(\alpha)}\mu_{ij}^{(\alpha)}F_j, \tag{5}$$

where $\mathbf{F}$ is the (uniform) applied electric field, $n^{(\alpha)}$ is the density of carriers in band α and we have defined the mobility tensor

$$\mu_{ij}^{(\alpha)} = \frac{2e}{\hbar n^{(\alpha)}} \int \frac{d\mathbf{k}}{(2\pi)^3} v_i^{(\alpha)}(\mathbf{k})\tau_i^{(\alpha)}(\mathbf{k}) \frac{\partial f^{(\alpha)}(\mathbf{k})}{\partial k_j}, \tag{6}$$

where $f^{(\alpha)}(\mathbf{k})$ is the distribution function in band or valley α.

The simplicity of Eq. (5) is deceiving: In fact we have not simplified at all the original transport equation, but have simply transferred its complexity into the non-linear integral equation Eq. (4). In order to proceed, we must consider separately the relaxation rates due to scattering with acoustic phonons on one side, and scattering with optical phonons and alloy scattering on the other. The relaxation rates associated with the latter processes can be simplified considerably: In bulk cubic materials and for strain applied along the [001] direction, we retain symmetry under reflections around the Cartesian planes, so that $v_i^{(\beta)}(\mathbf{k}')$ is an odd function of $\mathbf{k}'$. Nonpolar scattering with optical phonons has been shown to be 'momentum randomizing' (*i. e.*, the scattering kernel $S_{op}(\mathbf{k}'\beta;\mathbf{k}\alpha)$ is symmetric under inversions $\mathbf{k}' \rightarrow -\mathbf{k}'$), even in the highly anisotropic case of the valence bands[70,71]. A similar symmetry holds also for the conduction bands and for alloy scattering, and even under strain along the [001] direction. Therefore, also the relaxation time $\tau_i^{(\beta)}(\mathbf{k}')$ is an even function of $\mathbf{k}'$. The net result of these crucial simplifying considerations is that the 'in-scattering' terms represented by the numerator of the fraction in curly brackets in Eq.(4) disappear from the picture and now Eq. (4) reads:

$$\frac{1}{\tau^{(\alpha)}(\mathbf{k})} \simeq \sum_{\beta} \int \frac{d\mathbf{k}'}{(2\pi)^3} S(\mathbf{k}'\beta;\mathbf{k}\alpha), \tag{7}$$

having dropped the now unnecessary index i.

Scattering with acoustic phonons, on the other side, requires more drastic actions, since no simple symmetries of the scattering kernel can be invoked. On the contrary, Dür and co-workers have recently emphasized the anisotropy of the associated scattering rate[72]. Therefore, following what has now become standard practice, we embrace the equipartition and elastic approximations, justified by Lawaetz[70], Szmulowicz[71], and Hinckley *et al.*[11], among others, down to 150 K or so. In addition, we make a final approximation which amounts to looking for an iterative (fixed point) solution of the integral equation (4), but retaining only the the zero-th order term, that is, ignoring the presence of the factors $\tau_i^{(\alpha)}(\mathbf{k})$ and $\tau_i^{(\beta)}(\mathbf{k}')$ in the integrand of Eq. (4). The net result is that now we can write the relaxation time in the much simpler form:

$$\frac{1}{\tau_{ac,i}^{(\alpha)}(\mathbf{k})} = \sum_{\beta} \int \frac{d\mathbf{k}'}{(2\pi)^3} S_{ac}(\mathbf{k}'\beta;\mathbf{k}\alpha) \left\{ 1 - \frac{v_i^{(\beta)}(\mathbf{k}')}{v_i^{(\alpha)}(\mathbf{k})} \right\}. \tag{8}$$

The quality of this approximation has been shown by Lawaetz[70] to be excellent in the case of holes, since the even stronger approximation of isotropic scattering provides excellent results, as we shall discuss below. For electrons, Herring and Vogt[42] have analyzed this approximation in their Appendix A, concluding that the errors are not larger than a few percent. Taking explicitly into account the fact that we are interested in the Ohmic (linear) regime, we can approximate $f^{(\alpha)}(\mathbf{k})$ in Eq. (6) with its thermal equilibrium value, $f_0[E^{(\alpha)}(\mathbf{k})]$, and write:

$$\mu_{ij}^{(\alpha)} \simeq \frac{2e}{k_B T n^{(\alpha)}} \int \frac{d\mathbf{k}}{(2\pi)^3} v_i^{(\alpha)}(\mathbf{k}) v_j^{(\alpha)}(\mathbf{k}) \tau_i^{(\alpha)}(\mathbf{k}) f_0[E^{(\alpha)}(\mathbf{k})]. \tag{9}$$

Finally, the overall mobility will be given by the sum over all bands or valleys, weighted by the density, that is:

$$\mu_{ij} = \frac{1}{n} \sum_\alpha n^{(\alpha)} \mu_{ij}^{(\alpha)}, \tag{10}$$

where n is the total carrier density.

In order to evaluate numerically the mobility tensor, Eq. (9), it is convenient to split the discussion for electrons and holes, since we can benefit from different approximations.

A. Hole mobility

The numerical evaluation of Eq. (9) using the pseudopotential band-structure is both a forbidding and an unnecessary task. From these calculations we have already extracted the information we wanted, namely, the splitting of the bands as a function of strain and the uniaxial deformation potentials. Yet, the anisotropic and nonparabolic nature of the valence bands forces us to handle the integrals in Eqns. (7) or (8) and (9) accounting for these features. Therefore, we can turn to an easily manageable $\mathbf{k}\cdot\mathbf{p}$ approach, fitted to the pseudopotential results, since it represents an excellent approximation of the dispersion in the neighborhood of the Γ point. In this context, Bir and Pikus[73], Tiersten[49], Lawaetz[70], and Szmulowicz[71] have provided a general framework for handling the hole-phonon matrix element. We follow here the more agile notation of Ref. 11. Within the aforementioned elastic and equipartition approximation, the scattering kernel relative to the combined emission and absorption of acoustic phonons can be written as:[75]

$$S_{ac}(\mathbf{k}'\beta; \mathbf{k}\alpha) = \frac{2\pi k_B T}{\rho \hbar v_l^2} \left|\Delta_{ac}(\mathbf{k}'\beta; \mathbf{k}\alpha)\right|^2 \delta[E^{(\beta)}(\mathbf{k}') - E^{(\alpha)}(\mathbf{k})], \tag{11}$$

where the 'effective deformation potential' $\Delta_{ac}(\mathbf{k}'\beta; \mathbf{k}\alpha)$ accounts for the longitudinal and the two transverse phonon modes (labeled by the index η):

$$|\Delta_{ac}(\mathbf{k}'\beta;\mathbf{k}\alpha)|^2 = \sum_{\eta=1}^{3} \frac{v_l^2}{q^2 v_\eta^2} \sum_{i,j} \left| q_i < \mathbf{k}'\beta|\mathbf{D}_{ij}|\mathbf{k}\alpha > e_j^{(\eta)} \right|^2 . \tag{12}$$

Here v_l is the longitudinal sound velocity, v_η is the sound velocity associated with the polarization η, ρ is the lattice density, $\mathbf{q} = \mathbf{k} - \mathbf{k}'$ is the momentum transfer (*i. e.*, the phonon wavevector), and $\mathbf{e}^{(\eta)}$ is the polarization vector of mode η. On the $\mathbf{k}\cdot\mathbf{p}$-basis, the 6×6 matrices $\mathbf{D}$, functions of the deformation potentials a, b, and d, are given, for example, by Eq. (6) in Ref. 12. We have used for the phonon polarization vectors $\mathbf{e}^{(\eta)}$ the expressions given by Ehrenreich and Overhauser[76].

As far as scattering with optical phonons is concerned, we have[11,12,70,71]:

$$S_{op}(\mathbf{k}'\beta;\mathbf{k}\alpha) = \frac{3\pi d_0^2}{\rho a_0^2 \omega_{op}} \sum_{\eta=1}^{3} \sum_i \left| < \mathbf{k}'\beta|\mathbf{A}_i|\mathbf{k}\alpha > e_i^{(\eta)} \right|^2$$
$$\times (n_{op} + 1/2 \pm 1/2)\delta[E^{(\beta)}(\mathbf{k}') - E^{(\alpha)}(\mathbf{k}) \mp \hbar\omega_{op}], \tag{13}$$

where the upper and lower signs refer to emission and absorption processes, respectively, $\hbar\omega_{op}$ is the optical phonon energy, d_0 is the optical deformation potential, n_{op} the phonon occupation number, $\mathbf{e}^{(\eta)}$ the phonon polarization vectors. Similarly to the acoustic phonon deformation matrices, the 6×6 matrices $\mathbf{A}$ have been given in Ref. 12 (see Eq. (11) of this reference) on the the $\mathbf{k}\cdot\mathbf{p}$-basis, following Bir and Pikus[73].

We are now ready to evaluate the phonon-limited hole mobility from Eqns. (8) and (9). Let's rewrite the former as:

$$\frac{1}{\tau_i^{(\alpha)}(\mathbf{k})} = \sum_\beta \frac{1}{(2\pi)^3} \int_0^{2\pi} d\phi' \int_0^{\pi} d\theta' \sin\theta' \, \overline{k}(E_f,\theta',\phi') \left[1 - \frac{v^{(\beta)}(\mathbf{k}')}{v^{(\alpha)}(\mathbf{k})} \right] \frac{\widehat{S}(\mathbf{k}'\beta;\mathbf{k}\alpha)}{|\partial E_f/\partial k|_{k=\overline{k}}}, \tag{14}$$

where $\widehat{S}$ is the sum of the acoustic and optical scattering kernels 'stripped' of their energy-conserving δ-functions, which we have already eliminated with the integration over the radial coordinate in $\mathbf{k}$-space. The final quasi-momentum, $\mathbf{k}'$, of magnitude $\overline{k}(E_f,\theta',\phi')$, is obviously a function of the polar and azimuthal angles, θ' and ϕ', and of the final energy E_f. The numerical evaluation of Eq. (9) still amounts to performing a five-dimensional integral. A straightforward 'brute force' approach is out of the question. Therefore, we proceed in two ways: Either using a Monte Carlo sampling of the multi-dimensional integral, or using a 'constant matrix element' approximation in order to integrate analytically Eq. (14).

In the Monte Carlo evaluation of Eq. (9), in an 'outer' Monte Carlo loop, which samples the 3-dimensional integral Eq. (9), random vectors $\mathbf{k}$ are generated, uniformly distributed among the valence bands, with azimuthal angles ϕ uniformly distributed in $[0, 2\pi]$, polar angles such that $\cos\theta$ is uniformly distributed in $[-1, 1]$, and magnitude selected with probability distribution $f_0[E^{(\alpha)}(\mathbf{k})]$. During this Monte Carlo iteration, the carrier density in each band is also estimated. In a second, 'inner' loop, which samples Eq. (14), the relaxation rate for each of the generated $\mathbf{k}$ vectors is obtained by generating points $\mathbf{k}'$ uniformly distributed on the energy shell $E = E_f$. Typically, convergence is obtained after about 1000 'outer' loops of 1000 'inner' iterations each. Anticipating our results, using a valence band dilatation potential a and an optical deformation potential d_0 of 2.1 and 41.45 eV for Si, respectively, and 2.0 and 41.75 eV for Ge, we have obtained mobilities of 520 $\pm$ 9 cm^2/Vs for Si, 2076 $\pm$ 36 cm^2/Vs for Ge, corresponding to statistical errors of about 2.0% in both cases. The errors are estimated from the magnitude of the off-diagonal terms of the mobility tensor, which should vanish in absence of statistical noise.

Despite the satisfactory convergence, this Monte Carlo approach still requires intensive computational efforts. Therefore, some approximate way of estimating reliably the hole mobility would be desired. In his 1968 paper, Lawaetz[70] has noticed that adopting an isotropic phonon model characterized by an average sound velocity $\overline{v}_s^2 = (v_l^2 + 2v_t^2)/3$, averaging the acoustic-phonon/hole matrix element, Eq. (12), over equienergy surfaces, and adding the contributions of the three acoustic modes, one obtains an 'effective' acoustic phonon deformation potential, sometimes called E_{AC} (Ref. 10) or E_1 (Ref. 47), related to the quantity Ξ_{eff} of Ref. 70, given by (see also Ref. 73):

$$E_1^2 = \frac{\overline{v}_s^2}{v_l^2}\,\Xi_{eff}^2 \;=\; \frac{\overline{v}_s^2}{v_l^2}\left[a^2 + \frac{c_l}{c_t}\left(b^2 + \frac{1}{2}d^2\right)\right], \tag{15}$$

where $c_l = (3c_{11} + 2c_{12} + 4c_{44})/5$ and $c_t = (c_{11} - c_{12} + 3c_{44})/5$ are the average longitudinal and transverse elastic constants. According to Lawaetz[70], this expression, also employed in Refs. 10 and 47, should results in an error of less than 5% for the acoustic-phonon limited mobility. In the same 'isotropic spirit', we replace the overlap factors $|I(\mathbf{k}'\beta; \mathbf{k}\alpha)|^2$ by their angular averages, $< |I_{\alpha,\beta}|^2 >$, which are approximately equal to 1/2 for all interband processes and for intraband collisions within the two topmost bands, to unity for intraband transitions within the $v3$ bands. This allows us to simplify the acoustic-phonon contribution to Eq. (14) as follows:

$$\frac{1}{\tau_{ac}^{(\alpha)}(\mathbf{k})} \simeq \sum_\beta \theta(E - E^{(\beta)}) \frac{2^{1/2} m_{d,\beta}^{3/2}\ k_B T\ E_1^2}{\pi \rho \hbar^4 \overline{v}_s{}^2} < |I_{\alpha,\beta}|^2 > \ (E - E^{(\beta)})^{1/2}, \tag{16}$$

where the sum now runs over three bands β, accounting only for one spin state in each band, $\theta(x)$ is the step-function, E is the initial energy at $\mathbf{k}$, $E^{(\alpha)}(\mathbf{k})$, $E^{(\beta)}$ is the energy extremum of band β, and $m_{d,\beta}$ is the DOS effective mass defined by Eq. (3). Note that the index i has disappeared from the approximate expression Eq. (16) for the relaxation rate. Similarly, we follow Wiley[45], Costato and Reggiani[47], Takeda and co-workers[10], and approximate:

$$3\frac{d_0^2}{a_0^2}\sum_{\eta=1}^{3}\sum_i \left|<\mathbf{k}'\beta|\mathbf{A}_i|\mathbf{k}\alpha> e_i^{(\eta)}\right|^2 \simeq (DK)^2_{op}|I(\mathbf{k}'\beta;\mathbf{k}\alpha)|^2, \tag{17}$$

having set, for the general case of $Si_{1-x}Ge_x$ alloys:

$$(DK)^2_{op} = \frac{(1-x)M_{Si} + xM_{Ge}}{M_{Si}^{1-x}M_{Ge}^{x}}\frac{c_l + 2c_t}{\rho\overline{v}_s{}^2}\left(\frac{d_0}{a_0}\right)^2, \tag{18}$$

where $M_{Si} = 28.1088$ amu and $M_{Ge} = 72.7156$ amu are the atomic masses of Si and Ge. Once again, we replace the overlap integrals by their angular averages, so that the optical phonon contribution to Eq. (14) simplifies to:

$$\frac{1}{\tau_{op}^{(\alpha)}(\mathbf{k})} \simeq \sum_\beta \theta(E \mp \hbar\omega_{op} - E^{(\beta)})\frac{m_{d,\beta}^{3/2}(DK)^2_{op}}{2^{1/2}\pi\rho\hbar^3\omega_{op}}(E - E^{(\beta)} \mp \hbar\omega_{op})^{1/2}$$
$$\times(n_{op} + 1/2 \pm 1/2) < |I_{\alpha,\beta}|^2 > . \tag{19}$$

Note that these expressions are the 'usual' expression for the hole-phonon scattering rates employed in the Monte Carlo literature (see, for example, Refs. 21 and 60, 77–79). These isotropic, or 'constant hole-phonon matrix element', approximations have reduced the problem to the evaluation of a 3-dimensional integral, Eq. (9). Using about 10^4 **k**-points, and using the same deformation potentials, we obtain now for the trace of the hole mobility tensor values of 505 cm^2/Vs for Si and 2056 cm^2/Vs for Ge. For Si this is an error with respect to the Monte Carlo evaluation of about 3%, while for Ge it is an insignificant error which is even smaller than the statistical uncertainty in the Monte Carlo results. Even when the anisotropy of the valence bands is enhanced by strain, we have verified in a few cases that the quality of this isotropic approximation, while degrading somewhat, remains acceptable. This is not to say that we can ignore the anisotropy of the hole-phonon matrix, whose importance has been recently stressed by Dür, Unterrainer and Gornik[72]. Rather, in cases in which the carrier distribution is mostly isotropic, judiciously chosen angular-averaged quantities[10,47] have their merits. Thus, we conclude that Lawaetz's expectations[70] are confirmed, and we shall use the simpler isotropic relaxation time model in the rest of this work.

B. Electron mobility

The scattering kernel for the electron/acoustic-phonon interaction within the ellipsoidal conduction valleys of Si and Ge has been obtained by Herring and Vogt[42] by expanding the matrix element in spherical harmonics and retaining the leading terms. Accounting for emission and absorption processes, using again the elastic and equipartition approximations, and summing over all phonon modes η, we have:

$$S_{ac}(\mathbf{k}'\alpha;\mathbf{k}\alpha) = \sum_{\eta} \frac{2\pi k_B T}{\rho\hbar v_{\eta}^2} \Delta_{\eta}(\chi)^2 \delta[E^{(\alpha)}(\mathbf{k}') - E^{(\alpha)}(\mathbf{k})]. \tag{20}$$

In order to emphasize the similarity with models using simple deformation potentials, we have expressed this results in terms of an effective deformation potential, $\Delta_{\eta}(\chi)$, function only of the angle χ between the longitudinal axis of the valley and the wavevector $\mathbf{q} = \mathbf{k}' - \mathbf{k}$ of the emitted phonon. This is given by $\cos\chi = q/q_l$, where q_l is the projection of $\mathbf{q}$ on the longitudinal axis. The expressions for $\Delta_{\eta}(\chi)$ can be obtained by multiplying by $\rho v_{\eta}^2 V/k_B T$ the corresponding expressions for the matrix elements given by Herring and Vogt up to terms of order $\cos^6\chi$ (see Table V in Ref. 42).

Nonpolar intravalley scattering with optical phonon vanishes for the (mainly) s-type wavefunctions around the Δ minima, while for states in the α-th L valley we use once more the 'momentum randomizing' property of this process and the Herring-Vogt transformation. The resulting relaxation time is isotropic and it is given by the usual expression:

$$\frac{1}{\tau_{op}(E)} \simeq \frac{m_{d,\alpha}^{3/2}(DK)_{op}^2}{2^{1/2}\pi\hbar^3\rho\omega_{op}} (n_{op} + 1/2 \pm 1/2)(E \mp \hbar\omega_{op})^{1/2} \; [\, 1 + \; (5/2)\gamma \; (E \mp \hbar\omega_{op}) \,], \tag{21}$$

where γ is an isotropic nonparabolicity parameter which we assume to be 0.5 eV^{-1} for the Δ-valleys, 0.3 eV^{-1} for the L-valleys, ignoring any dependence on composition or strain. Intervalley scattering is also isotropic, in complete analogy to Eq. (21) above, as described in Ref. 78.

Employing now a Cartesian frame aligned with the principal axes of the ellipsoids, evaluating the total relaxation rate by adding the contributions of isotropic nonpolar optical scattering, Eq. (7), and of anisotropic acoustic-phonon scattering, Eq. (8), and inserting the resulting total relaxation time into Eq. (9), Herring and Vogt[42] find that the mobility tensor is diagonal in this frame. The diagonal elements, $\mu_{\lambda\lambda}$, where λ runs over the longitudinal and transverse directions, can be recast in a form close to the Kubo-Greenwood expression, using the Herring-Vogt[42,78] transformation to perform three-dimensional integrals in $\mathbf{k}$-space:

$$\mu_{\lambda\lambda}^{(\alpha)} = \frac{2e}{3k_B T n^{(\alpha)}} (m_{\lambda}^{(\alpha)})^{-1/2} \int_0^{\infty} dE E \rho^{(\alpha)}(E) \; \tau_{\lambda}^{(\alpha)}(E) \; f_0(E) \; (\, 1 + \gamma \; E/2 \,), \tag{22}$$

where the mass $m_\lambda^{(\alpha)}$ is the band-edge mass in valley α along the λ-th principal axis of the ellipsoid, $\rho^{(\alpha)}(E) = 2^{1/2} m_{d,\alpha}^{3/2} E^{1/2}/(\pi^2\hbar^3)$ is the (parabolic) density of states in valley α (including spin), and the density-of-states effective mass is given by $m_{d,\alpha} = (m_l m_{t,||} m_{t,\perp})^{1/3}$. The λ-th component of the relaxation rate due to intravalley acoustic phonons emission and absorption processes can be expressed as a sum over the squared matrix elements for each mode η, averaged over the final energy shell:

$$\frac{1}{\tau_{ac,\lambda}^{(\alpha)}(E)} \simeq \sum_\eta \frac{2^{1/2} m_{d,\alpha}^{3/2}\ k_B T \Delta_{\eta,\lambda}^{(\alpha)\ 2} E^{1/2}}{\pi v_\eta^2 \hbar^4 \rho} \, [1 + \ (5/2)\gamma\ E\ ]. \tag{23}$$

Here, the longitudinal, $\Delta_{\eta,l}^{(\alpha)}$, and transverse, $\Delta_{\eta,t,||}^{(\alpha)}$ and $\Delta_{\eta,t,\perp}^{(\alpha)}$, components of the deformation potential are obtained by using the Herring-Vogt transformation, by considering the initial state $\mathbf{k}$ on the equienergy shell $E(\mathbf{k}) = E$, averaging over all possible final angle θ' and ϕ' for the possible final states $\mathbf{k}'$ over the shell, and averaging over all possible angles, θ and ϕ, of the initial state. In the general case of strained materials with valleys characterized by two transverse masses defined above, $m_{t,||}$ and $m_{t,\perp}$, we have a cumbersome but trivial generalization of Eqns. (46) and (47) of Ref. 42:

$$\Delta_{\eta,l}^2 = \frac{3}{16\pi^2} \int_0^{2\pi} d\phi' \int_0^{2\pi} d\phi \int_0^{\pi} d\theta' \sin\theta' \int_0^{\pi} d\theta \sin\theta \cos^2\theta \left[1 - \frac{\cos\theta'}{\cos\theta}\right] \Delta_\eta(\chi)^2, \tag{24}$$

$$\Delta_{\eta,t,||}^2 = \frac{3}{32\pi^2} \int_0^{2\pi} d\phi' \int_0^{2\pi} d\phi \int_0^{\pi} d\theta' \sin\theta' \int_0^{\pi} d\theta \sin^3\theta \cos^2\phi \left[1 - \frac{\sin\theta' \cos\phi'}{\sin\theta\cos\phi}\right] \Delta_\eta(\chi)^2, \tag{25}$$

$$\Delta_{\eta,t,\perp}^2 = \frac{3}{32\pi^2} \int_0^{2\pi} d\phi' \int_0^{2\pi} d\phi \int_0^{\pi} d\theta' \sin\theta' \int_0^{\pi} d\theta \sin^3\theta \sin^2\phi \left[1 - \frac{\sin\theta' \sin\phi'}{\sin\theta\sin\phi}\right] \Delta_\eta(\chi)^2, \tag{26}$$

where the angle χ is given by:

$$\cos^2\chi = (\cos\theta - \cos\theta')^2 \times \tag{27}$$
$$\left[(\cos\theta - \cos\theta')^2 + \frac{m_{t,||}}{m_l}(\sin\theta\cos\phi - \sin\theta'\cos\phi')^2 + \frac{m_{t,\perp}}{m_l}(\sin\theta\sin\phi - \sin\theta'\sin\phi')^2\right]^{-1}.$$

These integrals have been tabulated in Ref. 42 in their simpler form obtained in the case of only one transverse mass. Here we have evaluated them numerically.

It is interesting to compare the results of this anisotropic model with the isotropic deformation potentials often used in the literature for unstrained Si and Ge. Clearly, there is no unique way of defining an average deformation potential. Since we are interested in a comparison with values used for unstrained materials, in the evaluation of the mobility along the [100] or [110] direction, and, finally, since in most Monte Carlo simulations only longitudinal acoustic phonons are considered, we have decided to define the following isotropic average, analogous to the expression for the effective hole/acoustic-phonon deformation potential, Ξ_{eff}, given by Eq. (15):

$$\Delta_{eff}^2 = m_c \left[\left(\frac{2\Delta_{LA,t}^2}{3m_t} + \frac{\Delta_{LA,l}^2}{3m_l} \right) + \frac{v_l^2}{v_t^2} \left(\frac{2\Delta_{TA,t}^2}{3m_t} + \frac{\Delta_{TA,l}^2}{3m_l} \right) \right], \tag{28}$$

having assumed only one transverse mass, as it is appropriate for unstrained materials. The conductivity masses along the [100] direction are $m_c = 3m_l m_t/(m_t + 2m_l)$ for both the Δ and the L valleys. The values we have obtained and those employed in the literature are shown in Table V. These isotropic, effective deformation potentials yield the correct mobility in unstrained Si and Ge by definition. Yet, even in strained materials, the errors are smaller than 20% for the values of strain considered here, in complete analogy with the observations we made above in the case of holes.

Defining formally a thermal average $< ... >$ so that Eq. (22) can be recast in the compact form $\mu_{\lambda\lambda}^{(\alpha)} =< \tau_\lambda^{(\alpha)} > /m_\lambda^{(\alpha)}$, the final expressions for the overall mobility along the [100] direction (which, incidentally, coincides with the mobility along the [110] direction under the approximation of a single transverse mass) can be written as the contribution due to the in-plane [100] Δ valleys, the out-of-plane [001] Δ valleys, the equivalent L valleys, and the (negligible in most cases) contribution of the conduction valley at Γ, with an in-plane effective mass $m_{\|}^{(\Gamma)}$. In the general case of two transverse masses in the Δ and L valleys we can write it as:

$$\begin{aligned}\mu_{[100]} = \sum_\alpha r_\alpha \frac{< \tau_x^{(\alpha)} >}{m_x^{(\alpha)}} &= 2r_{\Delta,(100)} \left(\frac{< \tau_l^{(\Delta)100} >}{m_l^{(\Delta)100}} + \frac{< \tau_{t,\|}^{(\Delta)100} >}{m_{t,\|}^{(\Delta)100}} \right) + 2r_{\Delta,(001)} \frac{< \tau_t^{(\Delta)001} >}{m_t^{(\Delta)001}} \\ &+ 4r_L \left(\frac{< \tau_l^{(L)} >}{3m_l^{(L)}} + \frac{< \tau_{t,\|}^{(L)} >}{2m_{t,\|}^{(L)}} + \frac{< \tau_{t,\perp}^{(L)} >}{6m_{t,\perp}^{(L)}} \right) + r_\Gamma \frac{< \tau_\|^{(\Gamma)} >}{m_\|^{(\Gamma)}},\end{aligned} \tag{29}$$

where the coefficients r_α are the density ratios for each of the valleys of the indicated symmetry, and the quantities τ_x and m_x are the relaxation times and masses along the Cartesian axis x. The Hall factor R_H is evaluated from the following generalization of the expression given in Ref. 42:

$$R_H = \frac{1}{\mu_{[100]}^2} \sum_\alpha r_\alpha \frac{< \tau_y^{(\alpha)} \tau_z^{(\alpha)} >}{m_y^{(\alpha)} m_z^{(\alpha)}}, \tag{30}$$

where the relaxation times and masses along the y and z axes are the projections of the associated longitudinal and transverse quantities along these axes, in analogy with Eq. (53) above.

C. Dilatation deformation potentials

Having set the framework for the calculation of the mobility, we now turn to the problem of determining the complete set of deformation potentials needed to proceed. In order to evaluate the electron mobility, we must determine the dilatation deformation potential Ξ_d and a large set of intervalley scattering parameters. As far as the latter are concerned, for the case of Si we employ the 'standard' set reported in Ref. 78, taken from Brunetti *et al.*[80], although other sets have also been used in the past (see, for example, the early work of Ref. 81), differing mainly in the strength of the g-type scattering processes. Below we shall discuss briefly the consequences of making a different choice. For Ge, we also use the set reported in Ref. 78, taken from Ref. 82. We then evaluate the 300 K electron mobility as a function of the dilatation deformation potential a, or, equivalently, Ξ_d. In Fig. 8(a) we show the ratio of the calculated mobility over the experimental value (about 1450 cm^2/Vs for Si, 3900 cm^2/Vs for Ge[36]) as a function of a in a way essentially identical to what is done in Figs. 5 and 6 of the work by Herring and Vogt[42]. This figure shows that the experimental value of the mobility can be obtained for two values of a. In the case of Si, the two possible values, a = -9.7 eV and 2.1 eV, correspond to $\Xi_d^{(\Delta)}$ = -10.7 eV and 1.1 eV, respectively. There is quite a confusion in the literature concerning the choice to be made, confusion to which, regrettably, we have also contributed. In the past we have chosen a large and negative value for Ξ_d (Ref. 83), also motivated by theoretical pseudo-rigid-ion results[40], (possibly affected by an incorrect interpolation scheme for the ionic potential at large wavelength[55]), and inconsistent experimental data: A striking example is provided by the fact that while values for a around 2 eV are usually reported for both Si and Ge, a value of -10.2 eV for Si can be extracted from the deformation potential data reported in Ref. 36, according the Laikhtman and Kiehl[84]. Similarly, a value $a = -12.7$ eV for Ge is also reported in Ref. 36. However, here we find that the opposite choice is mandatory, because of the strong connection between the electron and hole mobility implied by the linear relationship between a and $\Xi_d^{(\Delta)}$: The choice a = -9.7 eV implies such a strong hole/acoustic-phonon scattering, that the 300 K hole mobility would be severely underestimated: Even when ignoring altogether scattering with optical phonons (that is, setting d_0=0), we would obtain a room temperature hole mobility of only about 420 cm^2/Vs, exhibiting, in addition, a much too weak temperature dependence. Thus, we must chose a = 2.1 eV. This value not only agrees with the values usually reported in the literature[11,36,45,47], but also implies a value for $\Xi_d^{(\Delta)}$, 1.1 eV, which is in excellent agreement with the theoretical results by Van de Walle[5] and Yoder *et al.*[54,55]. Similar values for the deformation potentials have also been used successfully by Feenstra and Lutz[85] dealing with scattering from strain variations in Si/SiGe heterostructures. For Ge, the two possible values are a = -7.56 eV and 2.0 eV, corresponding to $\Xi_d^{(L)}$ = -14.0 eV and -4.43 eV, respectively. Unlike what we find for Si, the first value still leaves us some room to adjust the optical deformation potential d_0 in order to match the 300 K hole mobility: Chosing $d_0 \simeq 25$ eV, we obtain a value of about 2000 cm^2/Vs. However, this causes the hole mobility to exhibit a temperature dependence in strong disagreement with experimental results, increasing with decreasing temperature only as $T^{-1.85}$ in the neighborhood of room temperature, against the $T^{-2.33}$ observed experimentally. Thus, we are forced to chose $a = 2.0$ eV, which also is a value frequently reported[5,36,49,53]. It is perhaps ironic that the temperature dependence of the *hole* mobility dictates the choice for the deformation potential in the *conduction* band.

Having determined the deformation potential a, the only parameter we are free to vary in order to reproduce the 300 K hole mobilities is the optical deformation potential d_0. This has been studied in great detail by Lawaetz[70], Szmulowicz[71], and, more recently, by Hinckley and coworkers[12]. We obtain values of 41.45 eV for Si and 41.75 eV for Ge. The former is definitely larger than the best estimates given in Refs. 70 and 71, but falls within the range given in Ref. 12. Ultimately, the larger value we require here is due to the somewhat smaller contribution of the acoustic phonons, as implied by the value we have obtained for the deformation potential d. In this respect, our results is in agreement with the values found in by Hinckley and Singh[12] when using their parameter set C. On the other side, the value for Ge is in excellent agreement with previous estimates, as shown in Table IV. In Fig. 8 we also show the dependence of the hole mobility on the deformation potential a. Finally, in Fig. 9 we show the temperature dependence of the electron and hole phonon-limited mobilities calculated with the parameters we have just derived. Results are shown only for temperatures as low as 50 K, but at temperatures below about 100 K or so neither the elastic approximation for acoustic-phonon scattering nor the nondegenerate approximation we have employed are valid. Yet, concentrating our attention on the high-temperature (above 200 K or so), we see an excellent agreement with the approximate power laws, $\mu \propto T^{-\alpha}$, reported in Ref. 36. These are indicated by dashed lines for electrons, solid line for holes in the figure. Note that these power laws are only valid in the neighborhood of room temperature. Note also that, in the case of holes, we see clearly the effect of the nonparabolicity of the valence bands, which manifests itself in a 'bump' of the $d \log \mu / d \log T$ slope[60]. This is particularly evident in the case of Si, since the proximity of the split-off band induces stronger nonparabolic distortions than in Ge.

Despite the remark we just made, we should note that many uncertainties enter the determination of the dilatation deformation potentials: The experimental values of the 300 K mobility vary over a non-negligible range and our evaluation of the hole mobility is intrinsically affected by a 2-to-5% error, because of both the statistical noise in its Monte Carlo evaluation and the approximations employed within the 'constant matrix element' scheme. It is difficult to provide a reliable error estimate for our values of a, Ξ_d, or d_0. Clearly, the parameter a cannot be determined with a precision better than about 0.5 eV: Values close to 2.5 eV for Si, or 1.2 eV for Ge, as obtained with the model-solid approach by Van de Walle[5], would imply room temperature electron mobilities of about 1400 and 3950 cm^2/Vs, for Si and Ge, respectively, still well within the experimental uncertainty. Yet, d_0 is probably the parameter affected by the largest error, having been extracted at the end of a rather long chain of derivations. The scatter of the published room-temperature hole mobility data *per se* (480 to 505 cm^2/Vs for Si, 1800 to 2060 cm^2/Vs for Ge, as reported in Refs. 12, 36, 70, 71) implies an uncertainty on d_0 of about 15% for Si and 25% for Ge. Hinckley and coworkers[12] have come to similar error-estimates when considering the uncertainty on other deformation potentials and valence band parameters. We hope that at least this component of uncertainty is minimized in our work.

The overall set of deformation potentials we have employed is shown in Tables III-V. Comparison is also made not only with the previously mentioned theoretical and experimental data relative to deformation potentials, (from Refs. 1, 12, 36, 44, 46–55, 86), but, in Table V, also with the 'effective' deformation potentials obtained from fits to transport measurements with analytic[10,70,71], or Monte Carlo[21,60,77–79] algorithms. Here, we have obtained these 'effective' deformation potentials from Eqns. (15), (17), and (28), using, in the latter ones, the expressions given in Table V of Ref. 42. Note that in the literature quite often the overlap factors have been lumped into effective deformation potentials relative to hole-phonon scattering[10,21,45], so that, when comparing with those published results, one should divide our values by a factor approximately equal to $\sqrt{2}$.

IV. CARRIER MOBILITY IN STRAINED Si, Ge, AND SiGe ALLOYS

Having determined a consistent set of transport parameters (band structure, effective masses, and deformation potentials), we can now evaluate the low-field mobility in strained materials. We shall first discuss the mobility in strained Si and Ge, and move to SiGe alloys afterwards.

A. *Mobility in strained Si and Ge*

Figure 10 shows the electron (a) and hole (b) mobilities at 300 K in Si under strain along the [001] direction. The noise in the electron mobility curves should be attributed to the noise in the effective masses, as determined from the pseudopotential band structure. Hole mobilities, computed using the $\mathbf{k}\cdot\mathbf{p}$ band structure, are much smoother.

For biaxial tensile strain in the plane of the layer ($a_{||}/a_0 > 1$ in the figure), the in-plane electron mobility, $\mu_{||}$, increases sharply: Electrons populate the two lower energy Δ-valleys with longitudinal axis along the [001] directions. The lower conductivity mass $m_t^{(\Delta)001}$ (see Fig. 4(a)) is the obvious main cause of the increased mobility. Minor effects, somewhat canceling each other, are a small decrease of intervalley scattering (very moderate indeed, since the strong g-type process remains effective) and a slight increase of the conductivity mass. The electron mobility reaches a value of about 2300 cm^2/Vs, at a biaxial tensile strain about 1%, exceeding or close to recent experimental[19,26–28] results. However, the very large *Hall* mobilities observed by Ismail and co-workers[24,25,87] (exceeding 2700 cm^2/Vs) cannot be explained, since we have computed a Hall factor very close to unity ($\simeq$ 1.006) for Si under 1% biaxial tensile strain. (Note that for unstrained Si, we find an electron Hall factor of about 1.14, in excellent agreement with the experimental value of 1.15 reported by Morin and Maita[88]). Higher values of the electron mobility at 1% biaxial tensile strain can be obtained only by invoking intervalley scattering models which enhance the role of the f-scattering processes, such as those proposed by Canali *et al.*[81] and employed by Basu and Paul[31], or those (with equal strength for f- and g-scattering) by Vogelsang and Hofmann[19], since f-scattering becomes ineffective as the degeneracy of the $\Delta(100)$- $\Delta(001)$ valleys is lifted. Using the intervalley model of Ref. 81, we find a bulk (unstrained) mobility of about 1600 cm^2/Vs and a peak drift mobility in strained Si exceeding 3500 cm^2/Vs, as shown by the open triangles and deltas in Fig. 10(a). While this may be a pleasing result suggesting that we should favor the model of Ref. 81 over that of Ref. 80, we should recall that the former was modified by Brunetti and co-workers in order to explain experimental data on the field dependence of the diffusion constant. Unfortunately, we must view this as an open problem. In the following we shall adhere to the model of Ref. 80, but we should keep in mind the possibility that this choice may result in an underestimation of the electron mobility in some cases.

Under the same conditions, the 'out-of-plane' mobility, $\mu_\perp$, drops equally abruptly, since the conductivity mass is now the much higher longitudinal mass, $m_l^{(\Delta)001}$. Under strain of opposite sign, the in-plane mobility first decreases, as electrons populate mainly the 4 larger-conductivity-mass Δ-valleys with longitudinal axis along the [100] directions. But soon, the reduction of the transverse mass in these valleys ($m_{t,\perp}^{(\Delta)100}$ in Fig. 4(a)) causes a reduction of the scattering rates, thanks to a lower density-of-states effective mass, and the mobility increases again, although not so spectacularly. The out-of-plane mobility, controlled by the transverse mass, remains higher.

The hole mobility, on the other side, increases spectacularly for strain of either sign. Indeed the principal causes of the enhancement are the breaking of the degeneracy of the $v2$ and $v1$ valence bands at Γ and, the reduction of the conductivity mass. As seen in Figs. 1(a) and 7(a), both occur as soon as any strain is applied. Yet, differences remain: For biaxial tensile strain in the plane of the layer, the $v1$ band exhibits a much higher energy than the $v2$ band, while for strain of opposite sign the splitting of these two bands remains comparable to k_BT. Therefore, interband scattering is ineffective in the former case, resulting in a much larger mobility. Finally, we should note that the extremely large mobilities we calculate in heavily strained materials are not too meaningful from a practical perspective: Layers subject to such a high strain can only be grown up to very small thicknesses, if at all, before the strain will be relieved by the formation of dislocations and other defects. In very thin layers, size quantization effects must be accounted for, as done by Laikhtman and Kiehl[84], for example, and this usually results in lower mobilities.

Figure 11 illustrates the case of Ge under the same conditions. The situation is qualitatively similar, as far as the hole mobility is concerned. Note in Fig. 11(b) an anisotropy much larger than in Fig. 10(b), a direct consequence of the larger anisotropy of the valence bands. Stresses of opposite sign cause the in-plane and out-of-plane mobilities to exhibit opposite trends. The electron mobility, however, exhibits a noticeably more complicated behavior. For biaxial tensile in-plane strain, electrons begin to populate the conduction states at Γ, for all but the smallest strain. This results in a dramatic enhancement of the mobility, also due to the decreasing in-plane electron effective mass in the Γ_{7c} valleys: The masses along the [100] and [110] directions drop from 0.056 m_0 in unstrained Ge to about 0.044 m_0 at 3.3% tensile biaxial strain, while the out-of-plane mass (along the [001] direction) decreases even more sharply from the same value, 0.056 m_0 in unstrained Ge, to 0.023 m_0 at 3.3% tensile biaxial strain. Note, however, that the direct gap now closes fast and calculations for $a_{\|}/a_0$ larger than about 1.03 or so are not meaningful. For compressive in-plane strain, at first (strain smaller than 1% or so) the electrons populate mainly the L-valleys. But the energy separation between these and the $\Delta(100)$-valleys shrinks, as the energy of the minima at the Δ along the [100] directions decreases. The resulting larger intervalley scattering causes, in turn, a lower mobility. For a larger strain, the electrons settle in the $\Delta(100)$-valleys. The mobility now approaches a constant value, approximately equal to the Δ-valleys electron mobility in unstrained Ge, which we calculate to be about 1040 cm^2/Vs. This is about 20% larger than the value measured by Ahmad and co-workers[89], about 800 cm^2/Vs, obtained by applying hydrostatic pressure to Ge. Note that had we selected an interpolation for the pseudopotential resulting in values of $\Xi_d^{(\Delta)} + \Xi_u^{(\Delta)}/3 - a$ in good agreement with other theoretical results, we would have obtained a much smaller value for $\Xi_d^{(\Delta)}$, resulting in weaker scattering between acoustic phonons and electrons in the Δ valleys of Ge, and so in an even larger Δ-valley electron mobility, in worse disagreement with the experimental data.

B. Alloy scattering and mobility in SiGe alloys

Turning our attention to SiGe alloys, we must first account for yet another scattering process, namely, alloy scattering. This process is usually assumed to be caused by the disorder component of the crystal potential left out by the 'virtual crystal approximation'.[90] In the usual 'inner potential' model[91], (*i. e.*, scattering from hard spheres of 'suitable' radius, R_a, and depth ΔU), the scattering kernel associated with this process takes the form[90,92]:

$$S(\mathbf{k}'\beta;\mathbf{k}\alpha) = \frac{2\pi}{\hbar}\Omega_c x(1-x)\,|G(q)|^2\,\Delta U^2\,|I(\mathbf{k}'\beta;\mathbf{k}\alpha)|^2\,\delta[E^{(\alpha)}(\mathbf{k}) - E^{(\beta)}(\mathbf{k}')], \qquad (31)$$

where $\mathbf{q} = \mathbf{k}' - \mathbf{k}$ is the momentum transfer (mapped to the first Brillouin Zone in the case of intervalley scattering), Ω_c is the volume of the unit cell, ΔU is the effective depth of the scattering well whose radius has been taken to be equal to the radius of a sphere with volume equal to the unit cell (*i. e.*, $R_a = a_0[3/(16\pi)]^{1/3}$). Finally, $I(\mathbf{k}'\beta;\mathbf{k}\alpha)$ is the overlap integral between Bloch states of wavevectors $\mathbf{k}'$ and $\mathbf{k}$ in bands β and α, respectively, and the function $G(q)$ is the form factor of the hard sphere,

$$G(q) = 3\ \frac{\sin(qR_a) - (qR_a)\cos(qR_a)}{(qR_a)^3}. \tag{32}$$

The strong dependence of Eq. (31) on q (going roughly as $(qR_a)^{-4}$ at large q), will effectively suppress the possibility of intervalley scattering in almost all cases, the only exception being the g-type scattering (between the [100] and the [$\bar{1}$00] Δ-valleys), since their separation, approximately $0.3(2\pi/a_0)$, is small enough. Thus, it is appropriate to consider the long wavelength limit, approximate $G(q)$ with unity, consider the angular average of the Bloch overlap factor, and express the relaxation time for a carrier in band α with quasi-momentum $\hbar\mathbf{k}$ as:

$$\frac{1}{\tau^{(\alpha)}(\mathbf{k})} \simeq \sum_{\beta} \theta[E^{(\alpha)}(\mathbf{k}) - E^{(\beta)}]\frac{2\pi}{\hbar}\Omega_c x(1-x)\Delta U^2 \rho^{(\beta)}[E^{(\alpha)}(\mathbf{k})] < |I_{\alpha,\beta}|^2 >, \tag{33}$$

where $\rho^{(\beta)}(E)$ is the (nonparabolic) density of states (of both spins, for reasons discussed below) in band or valley β. In the case of holes, the sum extends over all bands β at Γ, the overlap factor being always 1/2, except for intraband transitions within the split-off ($v3$) band. In the case of electrons, only intravalley processes and the g-type process mentioned above should be considered, because of the small values of $G(q)$ at large q: For example, just looking at the form factor $G(q)$, we expect that f-type processes among Δ-valleys and $L-L$ processes will not contribute more than 2%, $\Delta - L$ processes no more than 1%. Therefore, the sum extends over either the initial valley α or, whenever the minima of the conduction bands are at Δ, over the initial and the 'opposite' valley. Finally, the overlap factor is approximately taken to be unity.

We should regard Eq. (31) as a semi-empirical expression, subject to many possible criticisms. For example, Singh and Bajaj[93] have argued that the depth ΔU of the scattering center should be a function of $\mathbf{k}$, in order to account for band-structure effects. Marsh[95] has argued against the assumption that the alloy composition is completely random, and has accounted for clustering effects. Finally, the selection of the scattering potential, and in particular its radius R_a, is clearly somewhat arbitrary. Indeed, Harrison and Hauser[94] have made a different choice, assuming R_a to be the nearest-neighbor distance $\sqrt{3}a_0/4$, obtaining an expression, quite commonly found in the III-V literature, corresponding to a relaxation rate larger by a factor $3(\pi/4)^2 \simeq 1.85$. We should also add that the literature is often unclear about the density of states actually used in Eq. (33) above, namely, for electrons whether intervalley scattering is considered or not, and whether both spin states are included or not[10,17,15]: We suspect that most frequently the density of states for either spin is used. We have adopted also this convention, as wrong as it may be, in a perhaps futile attempt of making a meaningful comparison with published data. Our skepticism originates from the fact that, in addition to the theoretical and numerical 'fuzzyness' of the parameter ΔU, often in dealing with holes the overlap factors are accounted for by lumping them into ΔU, as in Ref. 17, or the cell-volume Ω_c is replaced by the inverse atomic density, $1/N_0$, as in Ref. 15. In the former case, this would result in effective scattering potentials a factor $\sqrt{2}$ smaller then what would have been obtained using our expression, Eq. (33). The opposite is true in the latter case. By putting all these uncertainties together, all we can do is compare the published 'raw' numbers for the effective alloy scattering parameter ΔU, even when significant corrections should have been made. Finally, we have linearly interpolated the deformation potentials of Si and Ge when dealing with alloys, after having verified directly the satisfactory validity of this approximation.

In Fig. 12 we show the calculated electron and hole mobilities at 300 K as a function of Ge mole fraction in relaxed SiGe alloys. The experimental Hall mobility data by Busch and Vogt[96] and, for electrons, also by Glicksman[92] are also shown. Recent Hall mobility data for holes by Chen *et al.*[97] are relative to samples in which impurity scattering is significant, having a donor density of 10^{17} cm^{-3}, and are not reproduced here. Concerns arise from the fact that we compare calculated *drift* mobilities to measured *Hall* mobilities. As discussed by Li and coworkers[98], employing a ratio of 1 is not likely to result in major errors in the case of electrons. Our calculations indeed result in Hall factors ranging from 1.14 (Si) to 0.92 (Ge). For holes the situation is less clear: Improving somewhat the approximations described by Look[99], that is, by assuming isotropic relaxation times, as in Eqns. (16) and (19), but now accounting for the anisotropy of the valence bands while averaging them as in Eq. (6), we find Hall factors of about 1.11 for Si, 2.02 for Ge, about 30% and 20% larger, respectively, than the experimental data of 0.86 in Si (Ref. 100) and 1.7 in Ge (Ref. 88). This might be due to the isotropic approximation for the relaxation times. As large as these corrections might be, the noise affecting the experimental data and the uncertainty caused by the qualitative nature of the alloy scattering model we use are even larger. Therefore, we shall ignore the problem and refer to the aforementioned Ref. 97 for additional information, while keeping in mind that our estimates for the alloy scattering potentials are subject to large errors. Of one conclusion we can be certain: As can be seen in Fig. 12, the inclusion of alloy scattering is necessary to explain the experimental data. For electrons we have employed two different effective alloy scattering parameters as fitting quantities, one for electrons in the Δ valleys, ΔU_Δ, and one for the L valleys, ΔU_L. The former determines the mobility in the range of Ge mole fraction x in which the material is Si-like (with conduction band minima at Δ), the latter in the much narrower range ($x > 0.85$) in which a Ge-like behavior (conduction band minima at L) is seen. As shown in the figure, for $x < 0.85$ the best fit is obtained for $\Delta U_\Delta =$ 0.5 eV. This agrees rather nicely with the value of 0.46 eV reported by Glicksman[92] and, more recently, by Manku and Nathan[16]. Note, however, that Venkataraman and co-workers[101] report a much larger value (0.8 eV) in quantum wells, while Li *et al.*[98]

obtain a much smaller value (0.2 eV) determined from measurements in relaxed and coherently strained alloys. In the Ge-like range of Ge mole fraction, the data by Busch and Vogt[96] and by Glicksman[92] are in clear disagreement. A value of $\Delta U_L = 0.6$ eV is required to match Glicksman's data, while a fit to Busch and Vogt's data requires $\Delta U_L = 1.4$ eV.

From Busch and Vogt's hole mobility data we obtain a value of $\Delta U = 0.9 \pm 0.1$ eV, again somewhat larger than either the value (0.6 eV) reported by Li *et al.*[98] and Venkataraman and co-workers[101], or the value employed by Takeda and co-workers[10], who have assumed ΔU to be the difference between the energy gaps of Si and Ge. Even smaller is the value (either 0.35 or 0.27 eV, depending on the experimental data considered) employed in Ref. 17. This state of affairs is, unfortunately, what we must expect from the empirical origin of Eq. (31). In the following we shall use $\Delta U_\Delta = 0.5$ eV, $\Delta U_L = 0.6$ eV, for the conduction band, and $\Delta U = 0.8$ eV for the valence bands.

Having not too comfortably settled on a particular choice of alloy scattering parameters, we show in Figs. 13 and 14 the electron and hole mobilities in SiGe alloys grown on <001> Si (Fig. 13) and <001> Ge (Fig. 14) substrates. Note how all the mobility enhancement expected from the removal of valley/band degeneracy and reduced effective masses is negated by the strong alloy scattering. Only for the largest value of strain we do see any advantage. However, we must stress again the 'fuzziness' of the alloy scattering model we have to contend with: Comparing with previously published theoretical results, we note that the results shown in Fig. 13(b) without the inclusion of alloy scattering are in agreement with those of Ref. 11 and by Chun and Wang[15] with alloy scattering. This is expected, in view of the very small alloy scattering potential (0.2 eV) employed in Refs. 11 and 15. The mobility calculated by Manku and co-workers[17] using a larger alloy scattering potential (0.35 eV) are indeed closer to our results.

V. SUMMARY AND CONCLUSIONS

In summary, we have presented a consistent picture within which carrier mobilities in strained Si, Ge, and SiGe alloys can be computed using a minimal set of empirical parameters: Starting from the pseudopotentials of Si and Ge, we have been able to obtain band-structure, effective masses, and uniaxial deformation potentials which are in satisfactory-to-excellent agreement with experimental data and previous theoretical results. The only 'fitting' parameters required to obtain the 'correct' carrier mobilities in bulk Si and Ge - the dilatation and optical deformation potentials - have been determined. Once more, dilatation and, at least for Ge, optical deformation potentials are in excellent agreement with the available experimental and theoretical data, while the optical deformation potentials for Si is somewhat larger than previously reported. The major uncertainties affecting our results stem from the wide range of experimental values for the carrier mobilities.

Having so determined the required transport parameters, we have calculated the carrier mobilities in strained Si and Ge. We have found the expected large enhancement of the hole mobility in Si and Ge, thanks to the splitting of the degeneracy of the valence bands. This is probably the result of greatest practical significance, in light of the potential usefulness of fast p-channel devices in the complementary metal-oxide-semiconductor (CMOS) technology. On the other side, we have found only a moderate enhancement of the electron mobility in strained Si. This constitutes the major theoretical problem we have not been able to solve: Large experimental values exceeding 2700 cm^2/Vs can only be explained using a set of intervalley scattering parameters which, unfortunately, is inconsistent with the measured field dependence of the diffusion constant.

Finally, carrier mobilities in SiGe alloys appear to be completely dominated by alloy scattering. All the advantages we might have expected on the basis of degeneracy lifting are canceled by this strong scattering process.

Acknowledgments

Many ideas originate from preliminary work on the subject by J. P. Krusius and one of us (MVF)[102]. Stimulating discussions with K. Ismail, P. Mooney, S. Tiwari, and J. Welser are also acknowledged. One of us (MVF) is pleased to thank C. G. Van de Walle for help in clarifying the confusion about the different definitions of the strain tensor found in the literature.

References

[1] C. G. Van de Walle and R. M. Martin, *Phys. Rev. B.* **34**, 5621 (1986).
[2] M. Gell, *Phys. Rev. B.* **38**, 7535 (1988); **41**, 7611 (1990).
[3] P. Friedel, M. S. Hybertsen, and M. Schlüter, *Phys. Rev. B.* **39**, 7974 (1989).
[4] M. M. Rieger and P. Vogl, *Phys. Rev. B.* **48**, 14276 (1993).
[5] C. G. Van de Walle, *Phys. Rev. B.* **39**, 1871 (1989).
[6] S. Krishnamurthy, A. Sher, and A.-B. Chen, *Phys. Rev. B.* **33**, 1026 (1986).
[7] C. Tserbak, H. M. Polatoglou, and G. Theodorou, *Phys. Rev. B 47*, 7104 (1993).
[8] Q. M. Ma, K. L. Wang, and J. N. Schulman, *Phys. Rev. B 47*, 1936 (1993).
[9] Zhi-Zong Xu, *Phys. Rev. B 47*, 3642 (1993).
[10] K. Takeda, A. Taguchi, and M. Sakata, *J. Phys. C: Solid State Phys.* **16**, 2237 (1983).
[11] J. M. Hinckley and J. Singh, *Phys. Rev. B* **41**, 2912 (1990).
[12] J. M. Hinckley and J. Singh, *J. Appl. Phys.* **76**, 4192 (1994).
[13] D. K. Nayak and S. K. Chun, *Appl. Phys. Lett.* **64**, 2515 (1994).
[14] D. K. Nayak, J. C. S. Woo, J. S. Park, K. L. Wang, and K. P. MacWilliams, *Appl. Phys. Lett.* **62**, 2853 (1993).
[15] S. K. Chun and K. L. Wang, *IEEE Trans. Electron Devices* **39**, 2153 (1992).
[16] T. Manku and A. Nathan, *IEEE Trans. Electron Devices* **39**, 2082 (1992).
[17] T. Manku, J. M. McGregor, A. Nathan, D. J. Roulston, J.-P. Noel, and D. C. Houghton, *IEEE Trans. Electron Devices* **40**, 1990 (1993).
[18] Th. Vogelsang and K. R. Hofmann, *IEEE Trans. Electron Devices* **39**, 2641 (1992).
[19] Th. Vogelsang and K. R. Hofmann, *Appl. Phys. Lett.* **63**, 186 (1993).
[20] H. Miyata, T. Yamada, and D. K. Ferry, *Appl. Phys. Lett.* **62**, 2661 (1993).
[21] T. Yamada and D. K. Ferry, *Solid State Electron.* **38**, 881 (1995).
[22] J. R. Chelikowsky and M. L. Cohen, *Phys. Rev. B* **14**, 556 (1976).
[23] C. Smith and M. E. Jones, *Superlattices and Microstructures* **4**, 391 (1988).
[24] K. Ismail, B. S. Meyerson, and P. J. Wang, *Appl. Phys. Lett.* **58**, 2117 (1991).
[25] S. F. Nelson, K. Ismail, J. O. Chu, and B. S. Meyerson, *Appl. Phys. Lett.* **63**, 367 (1993).
[26] Y. J. Mii, Y. H. Xie, E. A. Fitzgerald, D. Monroe, F. A. Thiel, B. E. Weir, and L. C. Feldman, *Appl. Phys. Lett.* **59**, 1611 (1991).
[27] D. Monroe, Y. H. Xie, E. A. Fitzgerald, and P. J. Silverman, in *Semiconductor Heterostructures for Photonic and Electronic Applications Symposium 1993*, (Mater. Res. Soc., Boston, MA, 1993), p. 449.
[28] J. Welser, J. L. Hoyt, and J. F. Gibbons, *IEDM Tech. Dig. 1994*, p. 373.
[29] U. König, A. J. Boers, F. Schaffler, and E. Kasper, *Electron. Lett.* **28**, 160 (1992).
[30] F. Stern and S. E. Laux, *Appl. Phys. Lett.* **61**, 1110 (1992).
[31] P. K. Basu and S. K. Paul, *J. Appl. Phys.* **71**, 3617 (1993).
[32] K. Ismail, J. O. Chu, and B. S. Meyerson, *Appl. Phys. Lett.* **64**, 3124 (1994).
[33] We employ here the definition of the 'strain tensor' given, for example, by C. Kittel, *"Introduction to Solid State Physics"*, 4^{th} edition (John Wiley and Sons, New York, 1971) Ch. 4. According to this definition, the off-diagonal components, e_{ij}, of the

strain tensor are related to the off-diagonal components, $\delta_{ij}+\epsilon_{ij}$, of the 'deformation matrix' (mapping the coordinates of points in the unstrained lattice to those in the strained lattice) by $e_{ij} = \epsilon_{ij} + \epsilon_{ji}$. A different definition is sometimes used in the literature (*e.g.*, Refs 1 and 5), identifying the off-diagonal components of the strain tensor with those of the symmetrized deformation matrix, *i. e.*, $e_{ij} = (\epsilon_{ij} + \epsilon_{ji})/2$.

[34] R. A. Logan, J. M. Rowell, and F. A. Trumbore, *Phys. Rev.* **136**, A1751 (1964).

[35] O. H. Nielsen and R. M. Martin, *Phys. Rev. B.* **32**, 3792 (1985).

[36] *Landolt-Börnstein: Numerical Data and Functional Relationships in Science and Technology, Group III: Crystal and Solid State Physics*, Volume 17, Semiconductors, O. Madelung, M. Schulz, and H. Weiss Eds., Subvolume a: *Physics of Group IV Elements and III-V Compounds*, O. Madelung Ed. (Springer-Verlag, Berlin, 1982).

[37] Rigorous application of the rigid-ion approximation obviously requires the atomic volume Ω_a to be rescaled when handling strained Si, Ge, or alloys. Instead, we have kept Ω_a constant in interpolating of the local components of the pseudopotentials. In view of the questionable validity of the rigid-ion approximation in Si and Ge, this is a simple matter of convenience. Indeed note that the shear deformation potentials are insensitive to changes of the atomic volume, and the band-gap (dilatation) deformation potentials depend on the changes of $V_s(G)$ with normalizing volume, $\partial V_s(q)/\partial\Omega_a$ at $\mathbf{q} = \mathbf{G}$. Therefore, within the purely empirical pseudopotential context, practically identical results can be obtained by either using the slopes $\partial V_s(G)/\partial G$ we have used while keeping Ω_a fixed in Eq. (2), or using a different interpolation yielding rescaled slopes $(\partial V_s(G)/\partial G)_{rescaled} = \partial V_s(G)/\partial G - 3V_s(G)/G$, while rescaling Ω_a.

[38] S. Bednarek and U. Rössler, Phys. Rev. Lett. **48**, 1296 (1982).

[39] P. B. Allen and M. Cardona, *Phys. Rev. B.* **27**, 4760 (1983).

[40] M. V. Fischetti and J. H. Higman, in *Monte Carlo Device Simulation: Full Band and Beyond*, Karl Hess ed., (Kluwer Academic, Norwell, 1991), p. 123.

[41] M. A. Ball, *J. Phys. C* **8**, 3328 (1975); **15**, 3328 (1982).

[42] C. Herring and E. Vogt, *Phys. Rev.* **101**, 944 (1956).

[43] R. People, *Phys. Rev. B* **32**, 1405 (1985).

[44] I. Balslev, *Phys. Rev.* **143**, 636 (1966).

[45] J. D. Wiley, *Solid State Comm.* **8**, 1865 (1970).

[46] L. D. Laude, F. H. Pollak, and M. Cardona, *Phys. Rev. B* **3**, 2623 (1971).

[47] M. Costato and L. Reggiani, *Lett. Nuovo Cimento* **4**. 848 (1970); *Phys. Status Solidi (b)* **58**, 471 (1973).

[48] M. Cardona and F. H. Pollak, *Phys. Rev.* **142**, 530 (1966).

[49] M. Tiersten, *J. Phys. Chem. Sol.* **25**, 1151 (1964).

[50] M. Chandrasekhar and F. H. Pollak, *Phys. Rev. B* **15**, 2127 (1977).

[51] I. Balslev, *Phys. Lett.* **24A**, 113 (1967).

[52] C. Jacoboni and L. Reggiani, *Adv. Phys.* **28**, 493 (1979).

[53] E. V. Starikov and P. N. Shiktorov, *Opt. Quant. Electron.* **23**, S247 (1989).

[54] P. D. Yoder, V. D. Natoli, and R. M. Martin, *J. Appl. Phys* **73**, 4378 (1993).

[55] P. D. Yoder, Ph.D. Thesis, University of Illinois at Urbana-Champaign, 1994.

[56] J. F. Morar and P. E. Batson, *J. Vac. Sci. Technol. B* **10**, 2022 (1992).

[57] J. Weber and M. I. Aloso, *Phys. Rev. B* **40**, 5683 (1989).

[58] S. Tiwari and D. J. Frank, *Appl. Phys. Lett.* **60**, 630 (1992)
[59] D. V. Lang, R. People, J. C. Bean, and A. M. Sergent, *Appl. Phys. Lett.* **47**, 1333 (1985).
[60] G. Ottaviani, L. Reggiani, C. Canali, F. Nava, and A. Alberigi-Quaranta, *Phys. Rev. B* **12**, 3318 (1975)
[61] G. Dresselhaus, A. F. Kip, and C. Kittel, *Phys. Rev.* **98**, 368 (1955).
[62] M. Tiersten, *IBM J. Res. Dev.* **5**, 122 (1961).
[63] H. Nakagawa and S. Zukotynski, *Can. J. Phys.* **55**, 1485 (1977); **56**, 364 (1977)
[64] P. Lawaetz, *Phys. Rev. B* **4**, 3460 (1971)
[65] J. C. Hensel and G. Feher, *Phys. Rev.* **129**, 1041 (1963).
[66] T. Manku and A. Nathan, *J. Appl. Phys.* **73**, 1205 (1993).
[67] T. E. Whall, A. D. Plews, N. L. Mattey, and P. J. Phillips, *Appl. Phys. Lett.* **66**, 2725 (1995).
[68] S.-H. Song, D. C. Tsui, and F. F. Fang, *Solid State Comm.* **96**, 61 (1995).
[69] J.-P. Cheng, V. P. Kesan, D. A. Grutzmacher, and T. O. Sedgwick, *Appl. Phys. Lett.* **64**, 1681 (1994).
[70] P. Lawaetz, *Phys. Rev.* **174**, 867 (1968); **183**, 730 (1969).
[71] F. Szmulowicz, *Phys. Rev. B* **28**, 5943 (1983).
[72] M. Dür, K. Unterrainer, and E. Gornik, *Phys. Rev. B* **49**, 13991 (1994).
[73] G. L. Bir and G. E. Pikus, *Sov. Phys. - Solid State* **2**, 2039 (1961). English translation from *Fizika Tverdogo Tela* **2**, 2287 (1960).
[74] H. Ehrenreich and A. W. Overhauser, *Phys. Rev.* **104**, 331 (1956).
[75] F. L. Madarasz and F. Szmulowicz, *Phys. Rev. B* **24**, 4611 (1981).
[76] H. Ehrenreich and A. W. Overhauser, *Phys. Rev.* **104**, 331 (1956).
[77] L. Reggiani, C. Canali, F. Nava, and G. Ottaviani, *Phys. Rev. B* **16**, 2781 (1977).
[78] C. Jacoboni and L. Reggiani, *Rev. Mod. Phys.* **55**, 645 (1983).
[79] J. Dewey and M. Osman, *J. Appl. Phys.* **74**, 3219 (1993).
[80] R. Brunetti, C. Jacoboni, F. Nava, L. Reggiani, G. Bosman, and R. J. J. Zijlstra, *J. Appl. Phys.* **52**, 6713 (1981).
[81] C. Canali, C. Jacoboni, F. Nava, G. Ottaviani, and A. Alberigi-Quaranta, *Phys. Rev. B* **12**, 2265 (1975).
[82] C. Jacoboni, F. Nava, C. Canali, and G. Ottaviani, *Phys. Rev. B* **24**, 1014 (1981).
[83] M. V. Fischetti and S. E. Laux, *Phys. Rev. B* **48**, 2244 (1993).
[84] B. Laikhtman and R. A. Kiehl, *Phys. Rev. B* **47**, 10515 (1993).
[85] R. M. Feenstra and M. A. Lutz, *J. Appl. Phys.* **78**, 6091 (1995).
[86] B. Weber and M. Cardona, *Phys. Rev. B* **15**, 875 (1977).
[87] K. Ismail, S. F. Nelson, J. O. Chu, and B. S. Meyerson, *Appl. Phys. Lett.* **63**, 660 (1993).
[88] F. J. Morin and J. P. Maita, *Phys. Rev.* **96**, 988 (1954).
[89] C. N. Ahmad, A. R. Adams, and G. D. Pitts, *J. Phys. C* **12**, L379 (1979).
[90] L. Nordheim, *Ann. Physik* **9**, 607 (1931).
[91] N. F. Mott, *Proc. Cambridge Phil. Soc.*, **32**, 281 (1936).
[92] M. Glicksman, *Phys. Rev.* **111**, 125 (1958).
[93] J. Singh and K. K. Bajaj, *J. Appl. Phys.* **57**, 322 (1985).
[94] J. W. Harrison and J. R. Hauser, *Phys. Rev. B* **13**, 5347 (1976).

[95] J. H. Marsh, *Appl. Phys. Lett.* **41**, 732 (1982).
[96] G. Busch and O. Vogt, *Helv. Phys. Acta* **33**, 437 (1960).
[97] Y. C. Chen, S. H. Li, P. K. Bhattacharya, J. Singh, and J. M. Hinckley, *Appl. Phys. Lett.* **64**, 3110 (1994).
[98] S. H. Li, J. M. Hinckley, J. Singh, and P. K. Bhattacharya, *Appl. Phys. Lett.* **63**, 1393 (1993).
[99] D. C. Look, in *"Semiconductors and Semimetals"*, Vol. 19, R. K. Willardson and A. C. Beer eds. (Academic Press, New York, 1983), p. 127.
[100] G. W. Ludwig and R. L. Watters, *Phys. Rev.* **101**, 1699 (1956).
[101] V. Venkataraman, C. W. Liu, and J. C. Sturm, *Appl. Phys. Lett.* **63**, 2795 (1993).
[102] J. P. Krusius and M. V. Fischetti, "Band Structure Effects on Electron Transport in Strained Layer Ge_xSi_{1-x} Thin Films", IBM Research Report RC15089 10/27/89.

MATERIAL PARAMETERS

quantity	symbol	units	Si	Ge
lattice constant	a_0	Å	5.43	5.65
density	ρ	g/cm^3	2.33	5.32
longitudinal sound velocity	v_l	10^5 cm/s	9.0	5.31
transverse sound velocity	v_t	10^5 cm/s	5.41	3.61
elastic constants	c_{11}	10^{11} dyne/cm^2	16.577	12.853
	c_{12}	10^{11} dyne/cm^2	6.393	4.826
	c_{44}	10^{11} dyne/cm^2	7.962	6.680
Poisson ratio	ν		–0.28	–0.273
	D_{001}		0.771	0.751
	D_{111}		0.439	0.3716
valence band parameters	L	atomic units	–5.53	–30.53
		eV Å^2	–21.07	–116.32
	M	atomic units	–3.64	–4.64
		eV Å^2	–13.87	–17.68
	N	atomic units	–8.32	–33.64
		eV Å^2	–31.70	–128.17
optical phonon energy	$\hbar\omega_{op}$	meV	61.2	37.04
Γ_{7v}–Γ_{8v} spin–orbit splitting	Δ_{so}	meV	44	296

Table I. Material parameters employed in this work. All values are from the compilation of Ref. 36, with the exception of the valence band parameters L, M, and N, obtained by fitting the $\mathbf{k}\cdot\mathbf{p}$ theory of Ref. 61 to the nonlocal empirical pseudopotential structure of the valence band.

PSEUDOPOTENTIAL PARAMETERS

quantity	symbol	units	Si	Ge
cut–off energy	E_{cut}	Ry	8.00	8.00
form factors	$V_s(\sqrt{3})$	Ry	–0.263	–0.236
	$V_s(\sqrt{8})$	Ry	–0.040	0.019
	$V_s(\sqrt{11})$	Ry	0.033	0.056
interpolation coefficients for pseudopotential	a_1	atomic units	8.659814	23.31608
	a_2	atomic units	3.505847	2.523037
	a_3	atomic units	0.7218257	0.6763484
	a_4	atomic units	3.654774	1.150263
s–well depth	α_0	Ry	0.55	0.0
s–well energy–dependence	β_0		0.32	0.0
d–well depth	A_2	Ry	0.0	0.295
s–well radius	R_0	atomic units	2.0	
d–well radius	R_2	atomic units		2.312
spin–orbit coupling	μ		0.000157	0.00093
internal ionic displacement parameter	ζ		0.53	0.44

Table II. Parameters employed in the calculation of the band structures of Si and Ge using nonlocal empirical pseudopotentials with spin-orbit interaction. All values are from Ref. 22, with the exception of the cutoff energy, E_{cut}, chosen to allow about 100 to 120 plane waves, the form factor $V_s(\sqrt{3})$ for Ge, as explained in the text, of the spin-orbit coupling constant μ for Si, fitted to the experimental spin-orbit splitting of the valence bands at the Γ point, and of the internal displacement parameter ζ, from Ref. 1.

CALCULATED DEFORMATION POTENTIALS

(all quantities in eV)

	Si		Ge	
	present work	literature	present work	literature
b	–2.33	–1.5[a], –2.1[b], –2.2[c], –2.33[d] –2.12[e], –2.35[f], –2.58[g], –2.27[h]	–2.16	–2.1[i], –2.2[a], –2.08[d], –2.5[e,j], –2.55[f], –2.86[k], –3.11[h]
d	–4.75	–3.4[a], –4.85[b], –5.3[f,g], –3.69[h]	–6.06	–3.5[g,l], –4.4[a], –3.7[m] –4.5[j], –5.3[f], –4.65[h], –7.0[i]
$\Xi_u^{(\Delta)}$	10.5	8.86[e], 8.47[h], 9.2[f,m,n], 7.3[o], 9.29[d]	9.75	7.24[e], 7.46[h], 9.42[f], 10.20[d]
$\Xi_u^{(L)}$	18.0	16.14[f], 12.35[h], 6.5[o]	16.8	11.07[h], 15.13[f], 16.2[m], 15.9 to 19.3[p]
$\Xi_d^{(\Delta)}+\Xi_u^{(\Delta)}/3-a$	2.5	–0.77[e], 1.72[f], 1.79[h], 0.29[d] 1.5[b], 1.2 to 3.8[p], 4.3[m]	5.75	–0.9[e], 1.31[f], 1.34[h], –1.9[d]
$\Xi_d^{(L)}+\Xi_u^{(L)}/3-a$	–3.1	–2.84[h], –3.12[f], –3.65[d], –4.42[e]	–0.83	–1.82[h], –2.64[e], –2.78[f], –2.0[m], –5.17[d]

Table III. Uniaxial - or shear - deformation potentials extracted from the calculated shifts of the energy at symmetry points for Si and Ge under [100] and [111] strain. Comparison is made with previous theoretical and experimental results.

(a) Ref. 45
(b) Ref. 46
(c) Ref. 47
(d) Ref. 4
(e) Ref. 7
(f) Ref. 1
(g) Ref. 48
(h) Ref. 3
(i) Ref. 49
(j) Ref. 53
(k) Ref. 50
(l) Ref. 51
(m) Ref. 44
(n) Ref. 52
(o) Refs. 54, 55
(p) Ref. 36

DEFORMATION POTENTIALS FROM FITS TO MOBILITY

(all quantities in eV)

	Si		Ge	
	present work	literature	present work	literature
a	2.1	2.1[a,b], 2.46[c], 2.06[d]	2.0	1.24[c], 2.0[a,e], 2.09[f], –12.7[g], 1.39[d]
d_0	41.5	29.3[h,i], 26.6[j] 29.1 to 39.6[k]	41.75	40.0[h], 33 to 39[l], 40.25[m] 36.5 to 44.1[i], 38.4 to 42.8[k]
$\Xi_d^{(\Delta)}$	1.1	1.2[n], 1.13[c], 5[l]	4.5	–0.6[c]
$\Xi_d^{(L)}$	–7.0	5.5[n], –6.04[c]	–4.43	–12.3 to –10.5[l], –6.6[c]

Table IV. Deformation potentials obtained from fits to the electron and hole 300 K mobility in Si and Ge. Note that only one of a, $\Xi_d^{(\Delta)}$, or $\Xi_d^{(L)}$, is an independent fitting variable, the remaining two being related to it via Eq. (15) of Ref. 1 and the values of $\Xi_d + \Xi_u/3 - a$ shown in Table III.

(a) Ref. 45
(b) Ref. 47
(c) Ref. 5
(d) Ref. 3
(e) Ref. 49
(f) Ref. 53
(g) Ref. 86
(h) Ref. 11
(i) Ref. 71
(j) Ref. 78
(k) Ref. 12
(l) Ref. 36
(m) Ref. 70
(n) Ref. 55

EFFECTIVE DEFORMATION POTENTIALS

(all in eV, except for $(DK)_{op}$, expressed in eV/Å)

	Si		Ge	
	present work	literature	present work	literature
Effective deformation potentials entering the carrier–phonon matrix elements:				
E_1 (Γ_v)	5.39	3.1[a], 5.0[b,c], 6.2[d]	6.49	3.66[a], 4.6[d,e]
$(DK)_{op}$ (Γ_v)	13.24	5.0[f], 9.05[a], 10.5[c]	12.17	8.65[a], 9.0[e], 16[c]
Δ_{eff} (Δ_{6c})	10.57	9.0[b]	9.58	9.0[b]
Δ_{eff} (L_{6c})	8.96		8.84	11.0[b]
Input from the literature: all intervalley processes from Ref. 83 and:				
$(DK)_{op}$ (L_{6c})	2.2[g]		5.5[b]	
Δ_{ac} (Γ_{7c})			5.0[b]	

Table V. Effective deformation potentials obtained by taking the average over angles and phonon modes of the anisotropic quantities shown in Tables III and IV. Comparison is made with isotropic effective deformation potentials used in the literature.

(a) Ref. 10 (c) Ref. 21 (e) Ref. 77 (g) Ref. 40
(b) Ref. 78 (d) Ref. 79 (f) Ref. 60

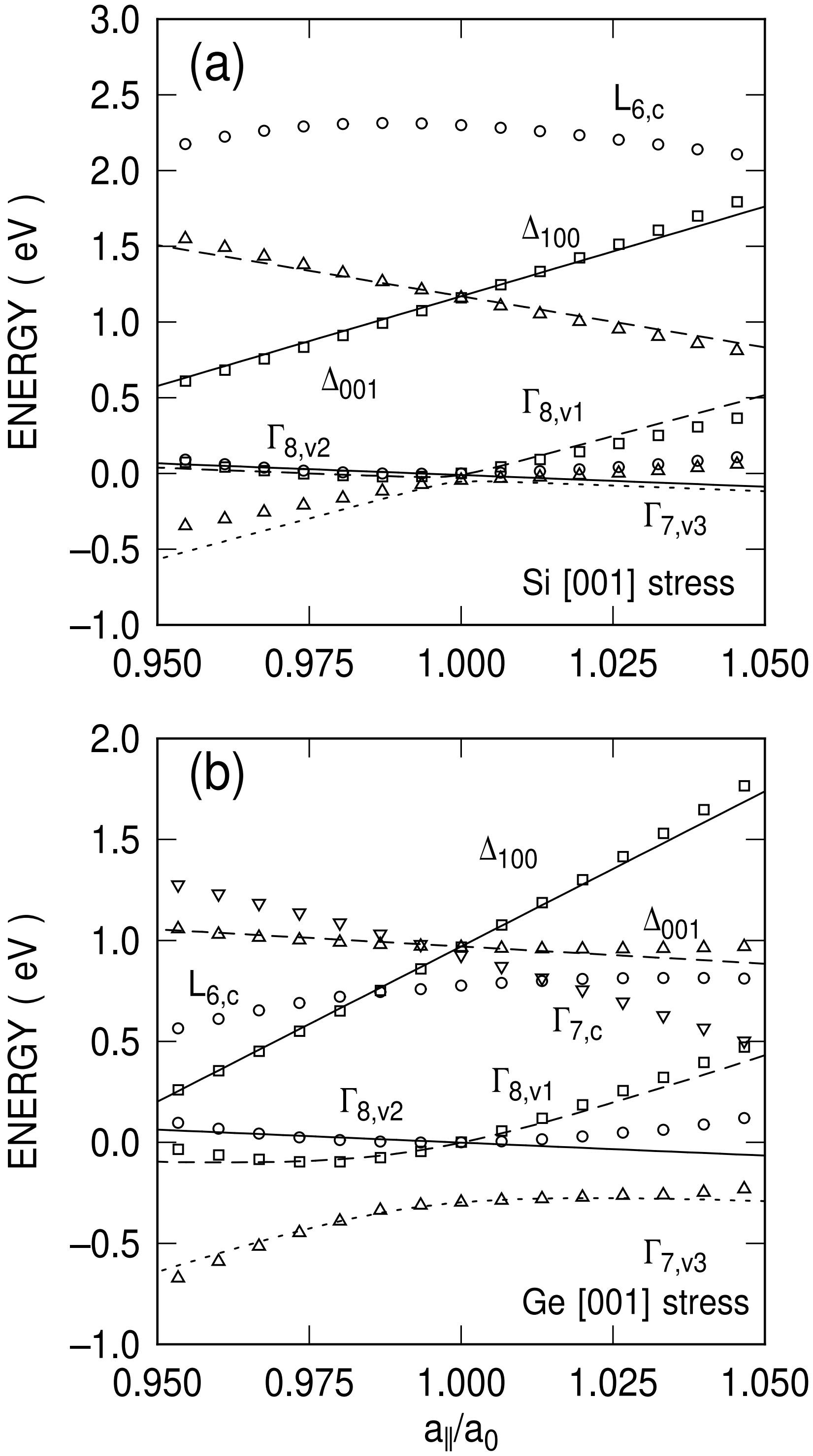

Fig. 1: Calculated valence and conduction band shifts at various symmetry points in Si (a) and Ge (b) as a function of in-plane biaxial strain $a_{\|}/a_0 - 1$. The energy scale has been fixed by setting arbitrarily to zero the top of the valence bands at zero strain, and using a valence band dilatation deformation potential $a = 2.1$ eV (Si) and 2.0 eV (Ge).

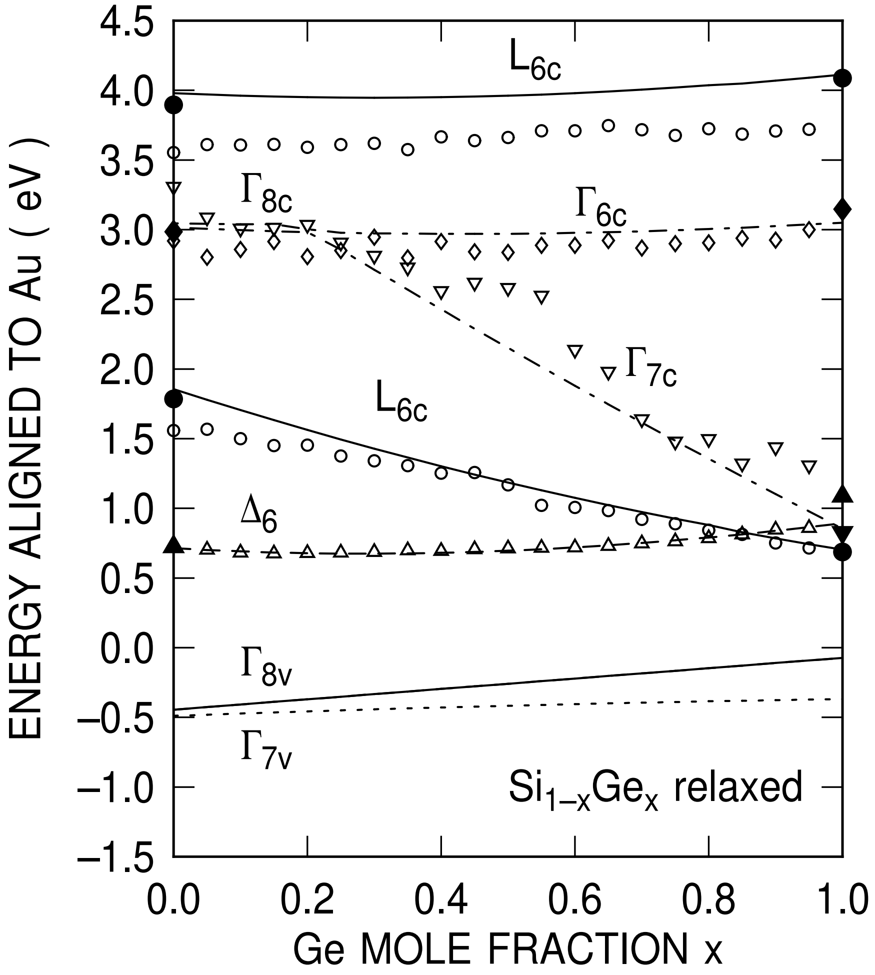

Fig. 2: Valence and conduction band shifts at various symmetry points for relaxed $\mathrm{Si}_{1-x}\mathrm{Ge}_x$ alloy as a function of Ge mole fraction. The lines show the results of nonlocal empirical pseudopotential band structure calculations, the open symbols the experimental results from Ref. 56, combined with the experimental data for the energy gap from Ref. 57 (open triangles for $x < 0.85$, circles for $x > 0.85$). The solid symbols are the experimental values for the energies at symmetry points in pure Si and Ge, as reported in Ref. 22.

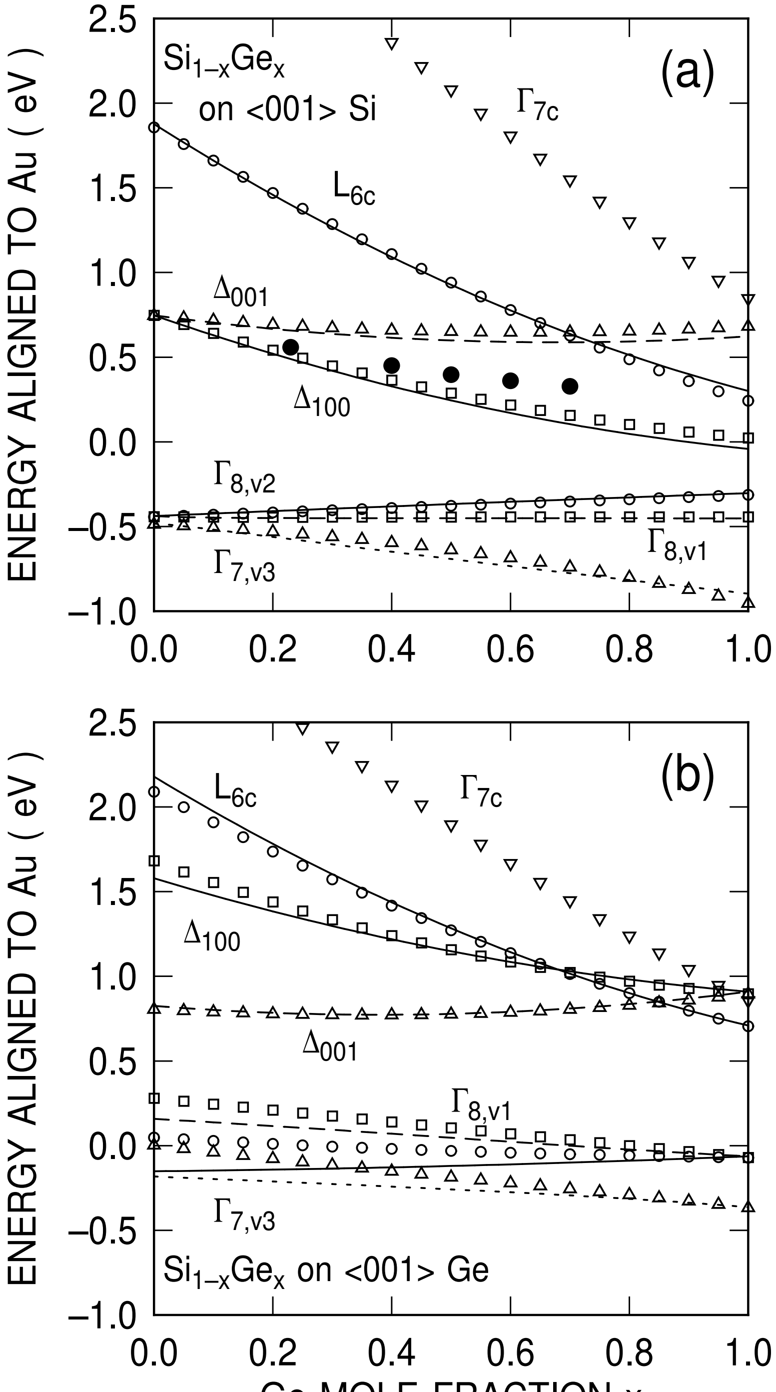

Fig. 3: Calculated valence and conduction band shifts at various symmetry points for $Si_{1-x}Ge_x$ alloys grown on a <001> Si substrate (a), and for $Si_{1-x}Ge_x$ alloys grown on a <001> Ge substrate (b), as a function of Ge mole fraction. The solid symbols in (a) are experimental results concerning the band-gap dependence on Ge composition, from Ref. 59.

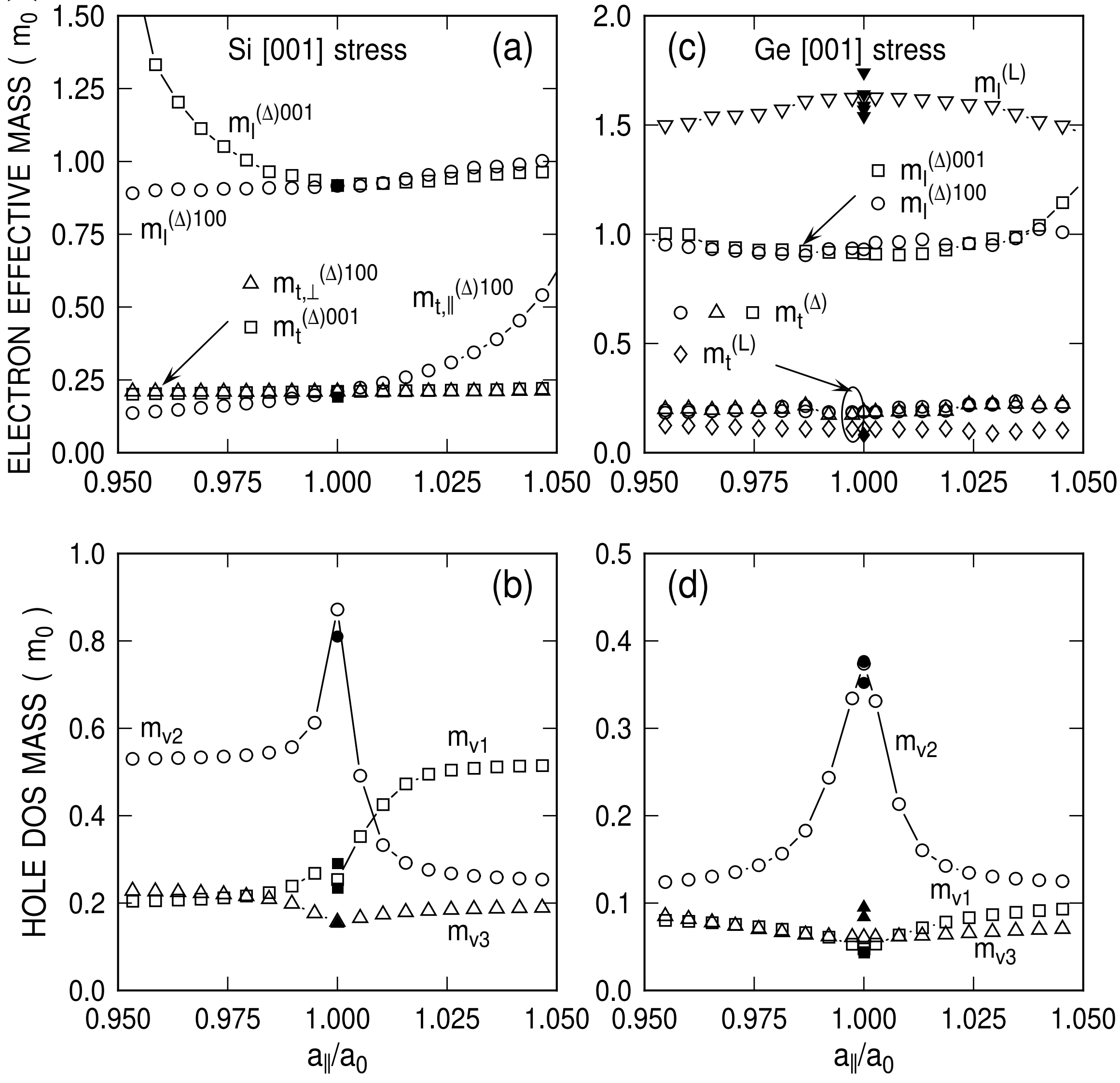

Fig. 4: Calculated curvature electron masses (open symbols,(a) and (c)) and hole density-of-states effective masses (open symbols, (b) and (d)), as a function of biaxial in-plane strain, corresponding to the situations of Fig. 1. Electron masses are 'curvature' masses, while for holes the density-of-states mass at the thermal energy is shown as discussed in the text. The solid symbols are experimental results from the compilation of Ref. 36.

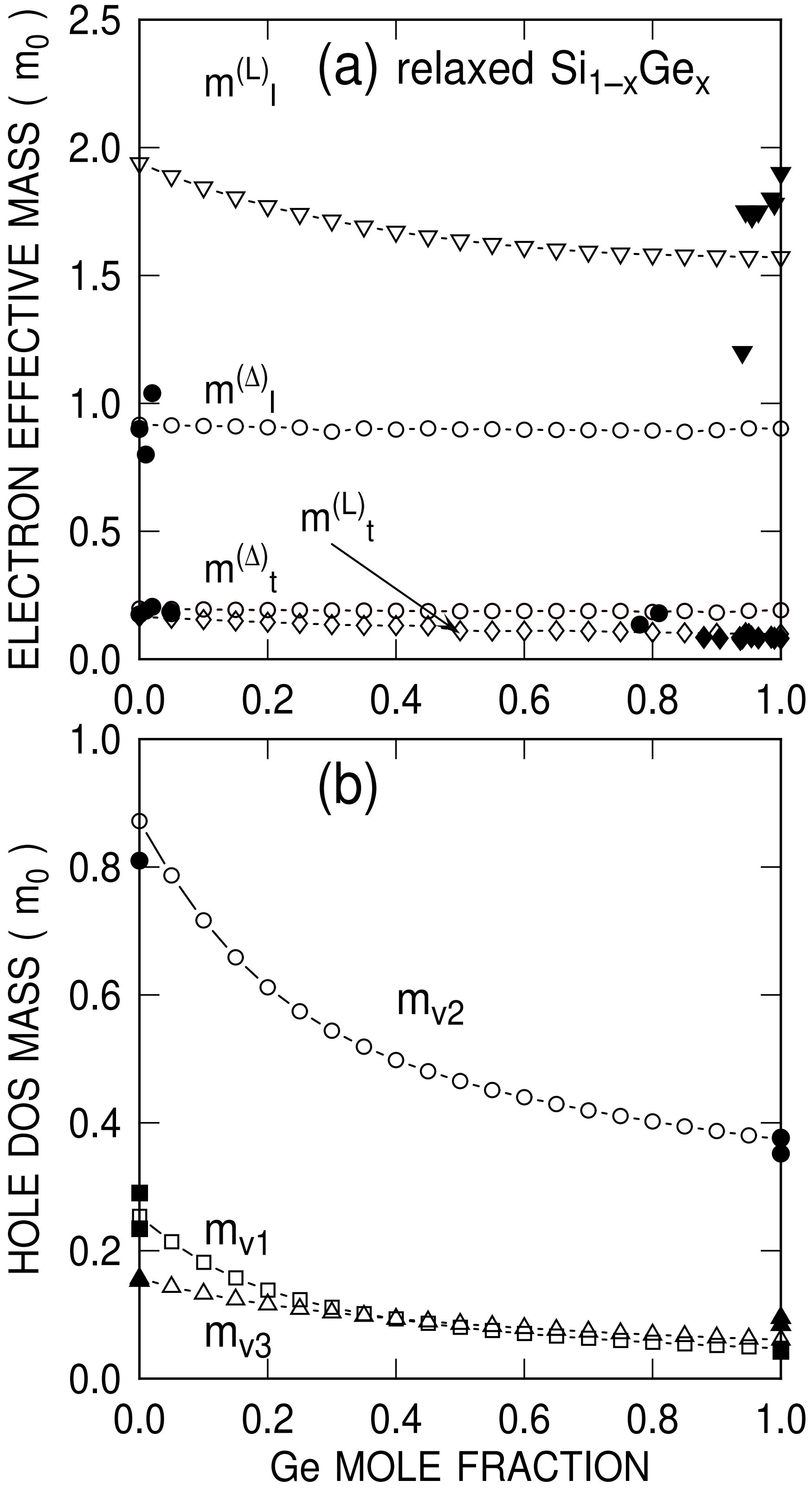

Fig. 5: Calculated (open symbols, as in Fig. 4) and experimental (solid symbols, from Ref. 36) electron (a) and hole (b) effective masses corresponding to the situations of Fig. 2.

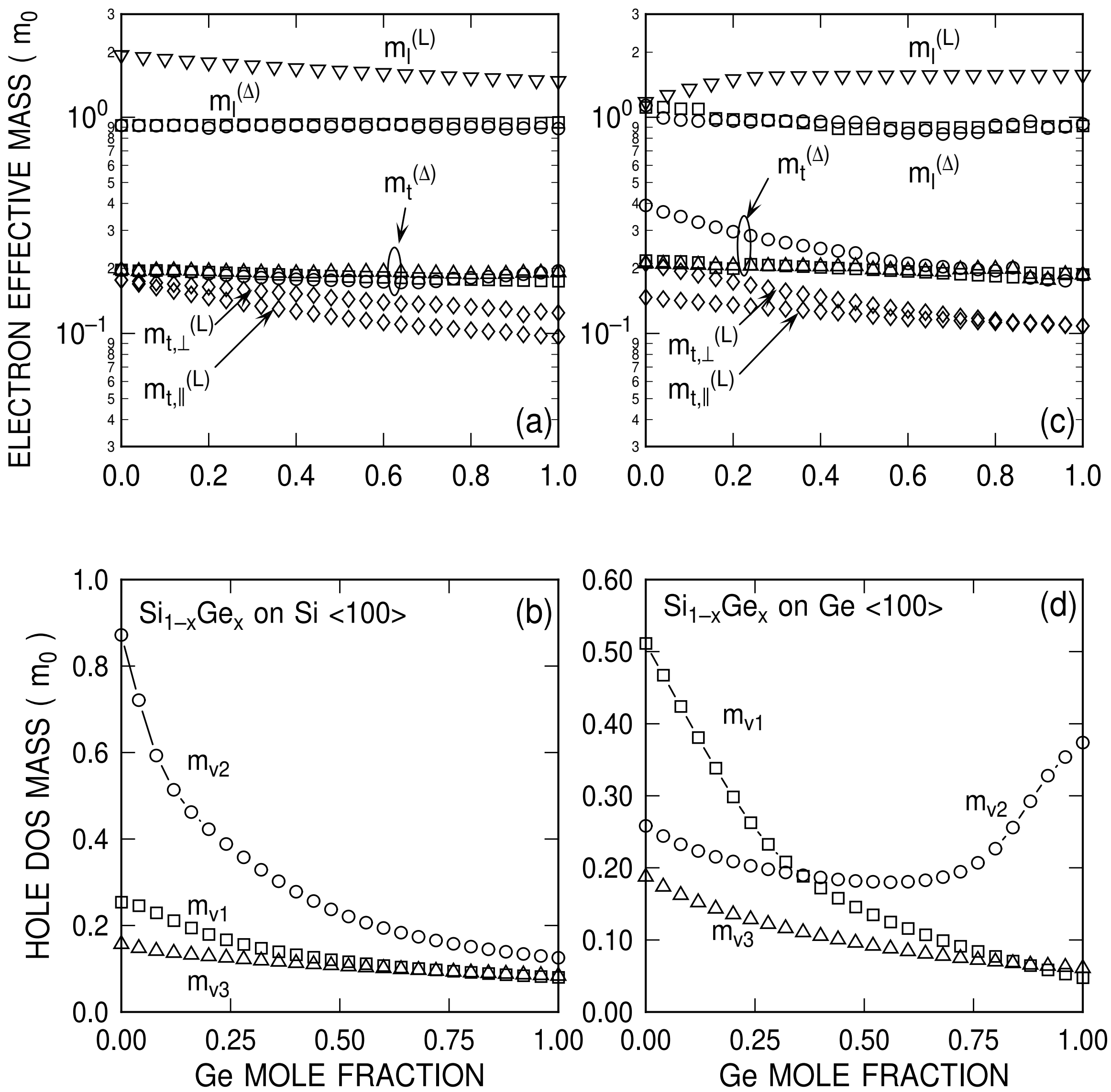

Fig. 6: Calculated electron, (a) and (c), and hole, (b) and (d) effective masses corresponding to the situations of Fig. 3. The meaning of the symbols, when not explicitly indicated, is as in Fig. 4.

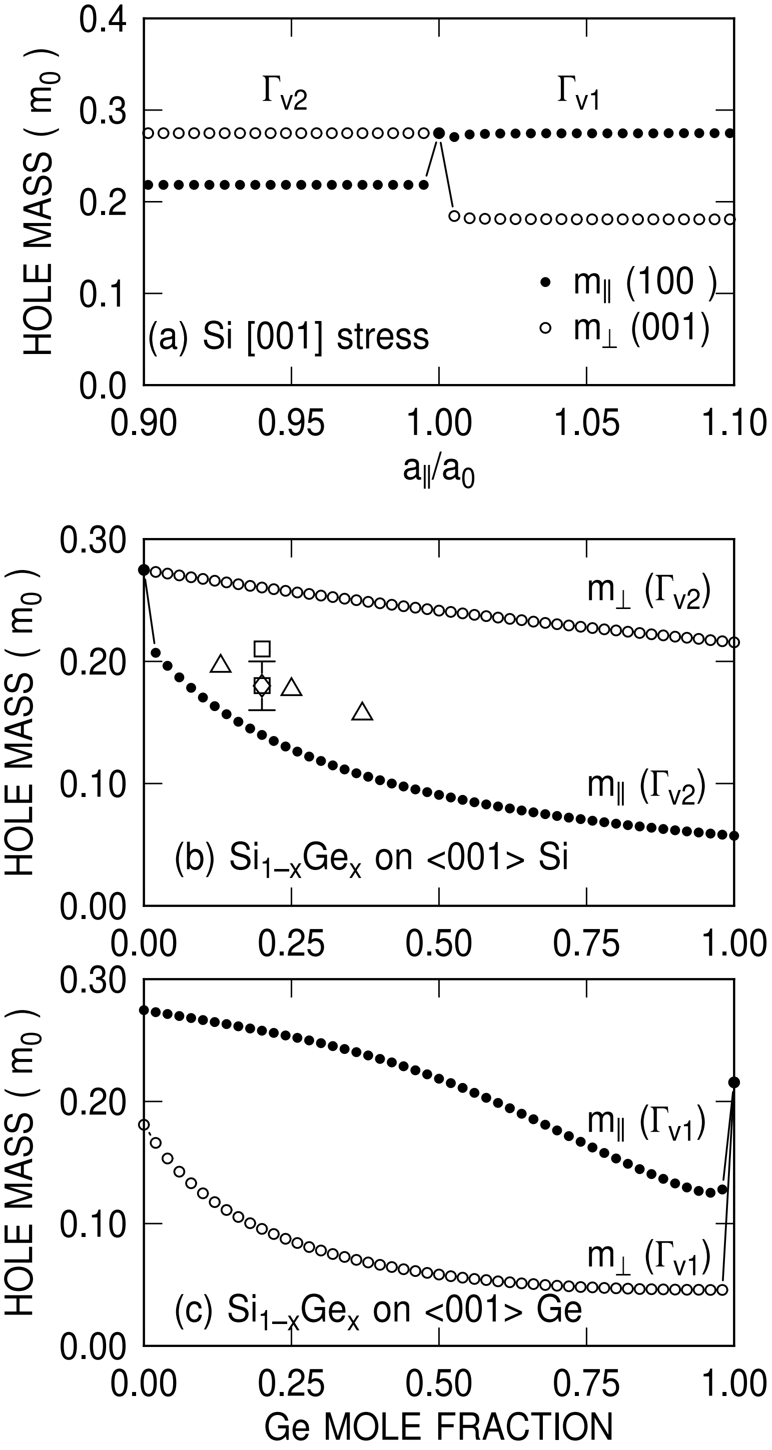

Fig. 7: Calculated band-edge masses for the topmost valence band in [001]-strained Si (a), $Si_{1-x}Ge_x$ alloys grown on <001> Si substrates (b), and $Si_{1-x}Ge_x$ alloys grown on <001> Ge substrates (c). The 'in-plane' (open symbols) and 'normal' (solid symbols) conductivity masses are shown. For $Si_{1-x}Ge_x$ on <001> Si we also show the extrapolated band-edge data by Cheng *et al.* (Ref. 69, open triangles), and the extrapolated zero-magnetic field masses reported by Whall and co-workers (Ref. 67, open square) and by Song *et al.* (Ref. 68, open diamond with error bar).

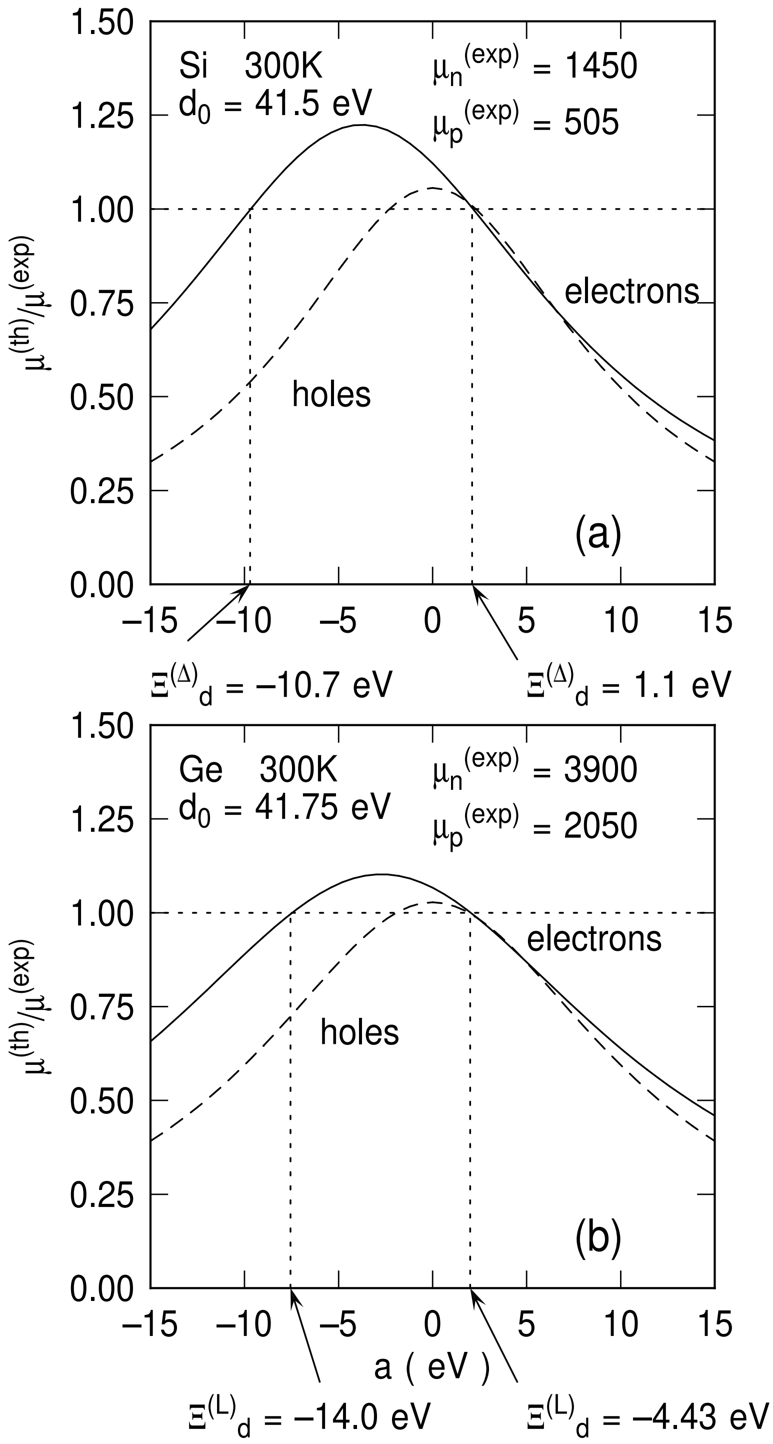

Fig. 8: Calculated trace of the 300 K phonon-limited electron (solid lines) and hole (dashed lines) mobility tensors (normalized to their experimental values) in bulk, unstrained Si (a) and Ge (b) as a function of the valence-band dilatation deformation potential a, which is related to the conduction-band dilatation deformation potential Ξ_d via Eq. (15) of Ref. 1.

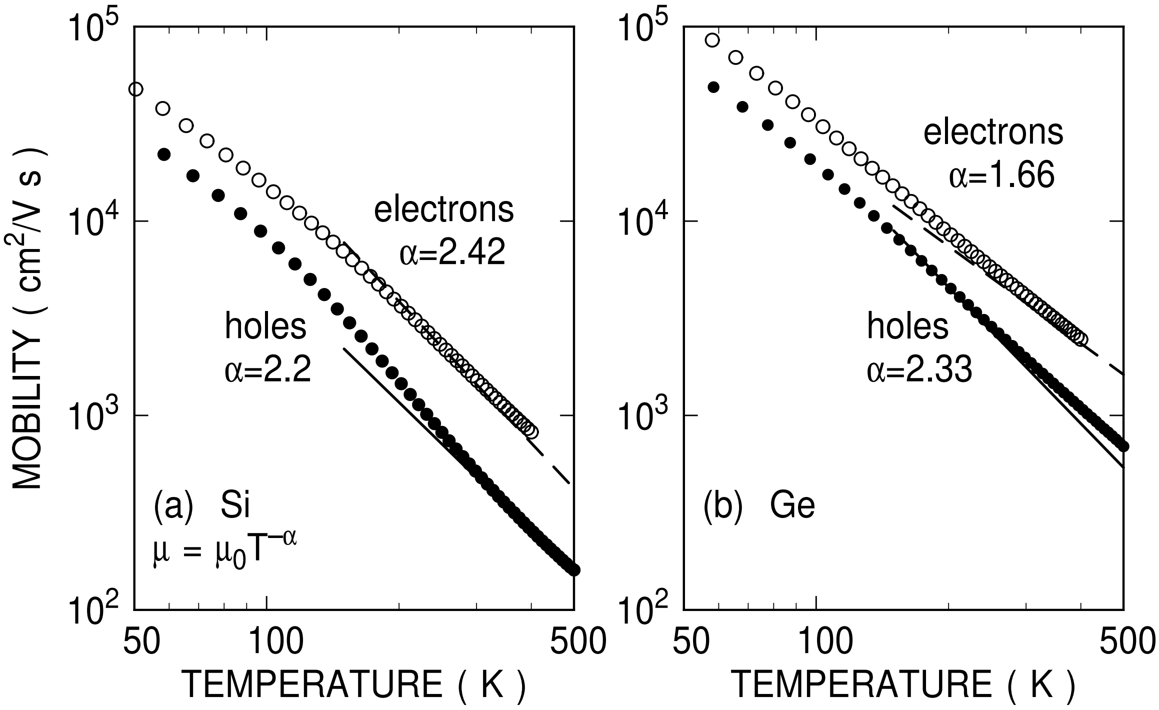

Fig. 9: Calculated temperature dependence of the phonon-limited electron (open symbols) and hole (solid symbols) mobility tensors in bulk, unstrained Si (a) and Ge (b). The dashed (electrons) and solid (holes) lines are power laws fitting experimental data in the neighborhood of room temperature only, taken from Ref. 36.

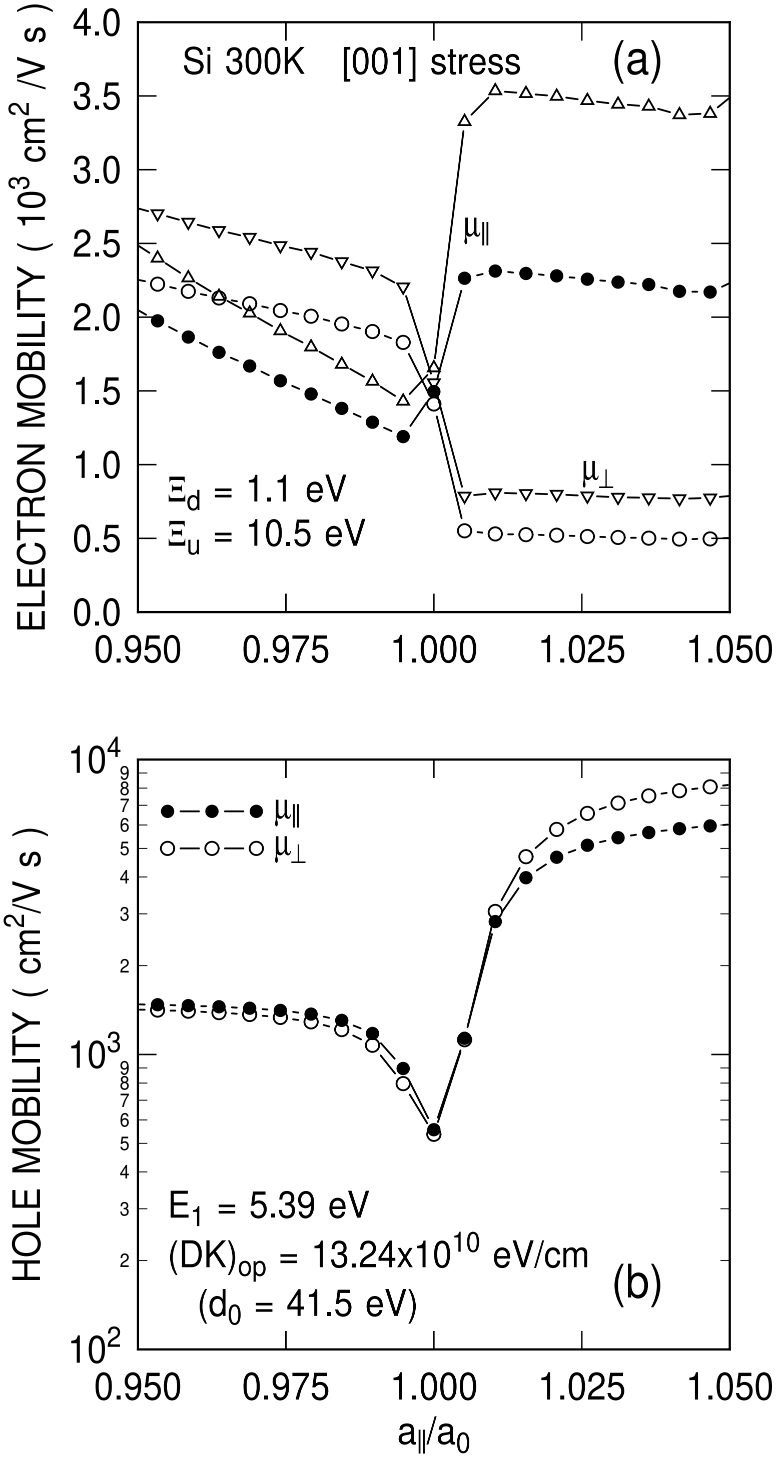

Fig. 10: Calculated phonon-limited 300 K electron (a) and hole (b) low-field mobility in Si under strain in the [001] direction. The dots, labeled $\mu_\parallel$, refer to the 'in-plane' mobility along the [100] and [110] directions, the circles, labeled $\mu_\perp$, refer to the mobility along the z-axis (the [001] direction), direction normal to the plane of the layer. The results indicated by open triangles and inverted triangles have been obtained using the intervalley deformation potentials of Ref. 81.

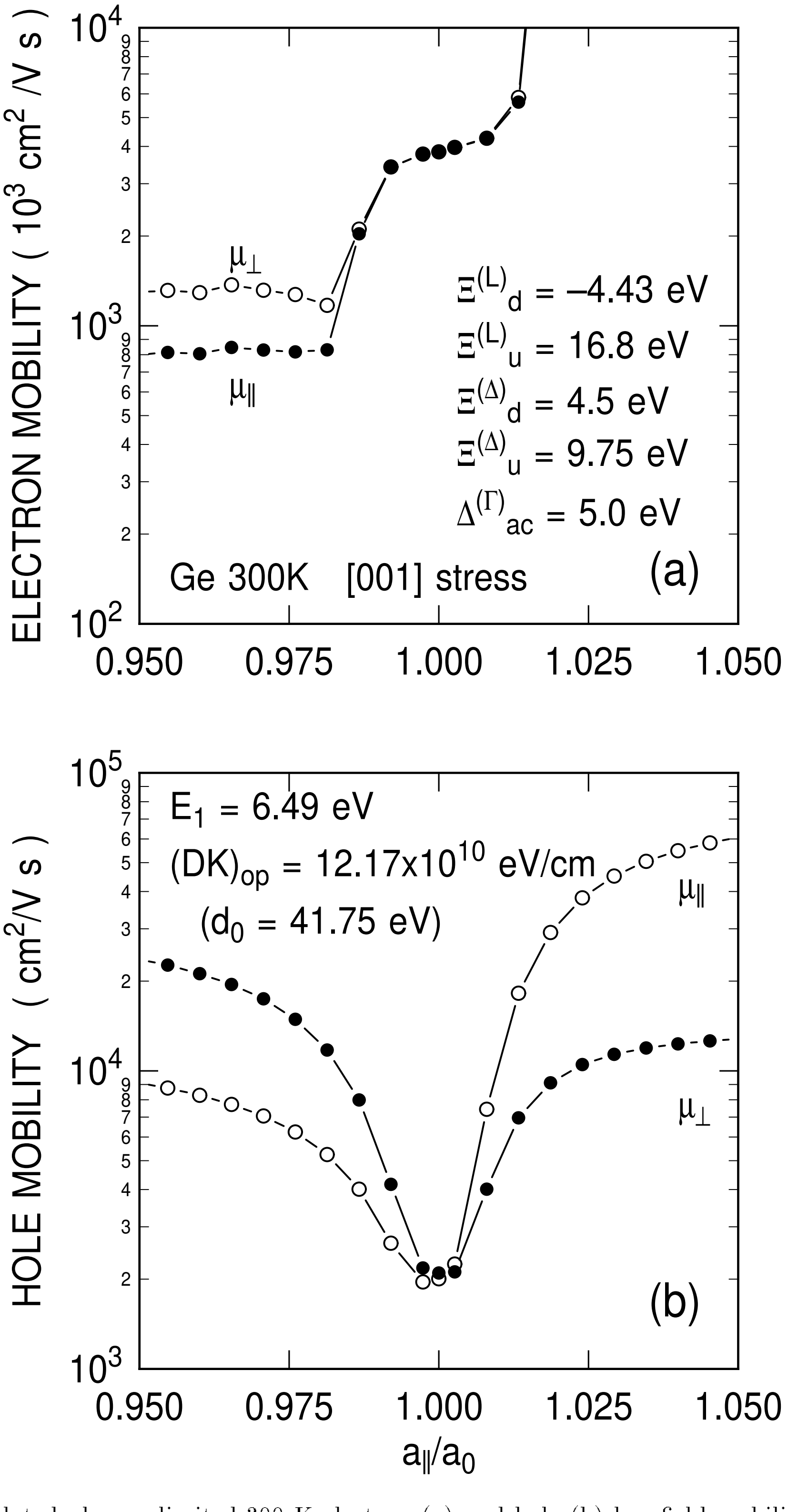

Fig. 11: Calculated phonon-limited 300 K electron (a) and hole (b) low-field mobility in Ge under strain in the [001] direction, as in Fig. 10.

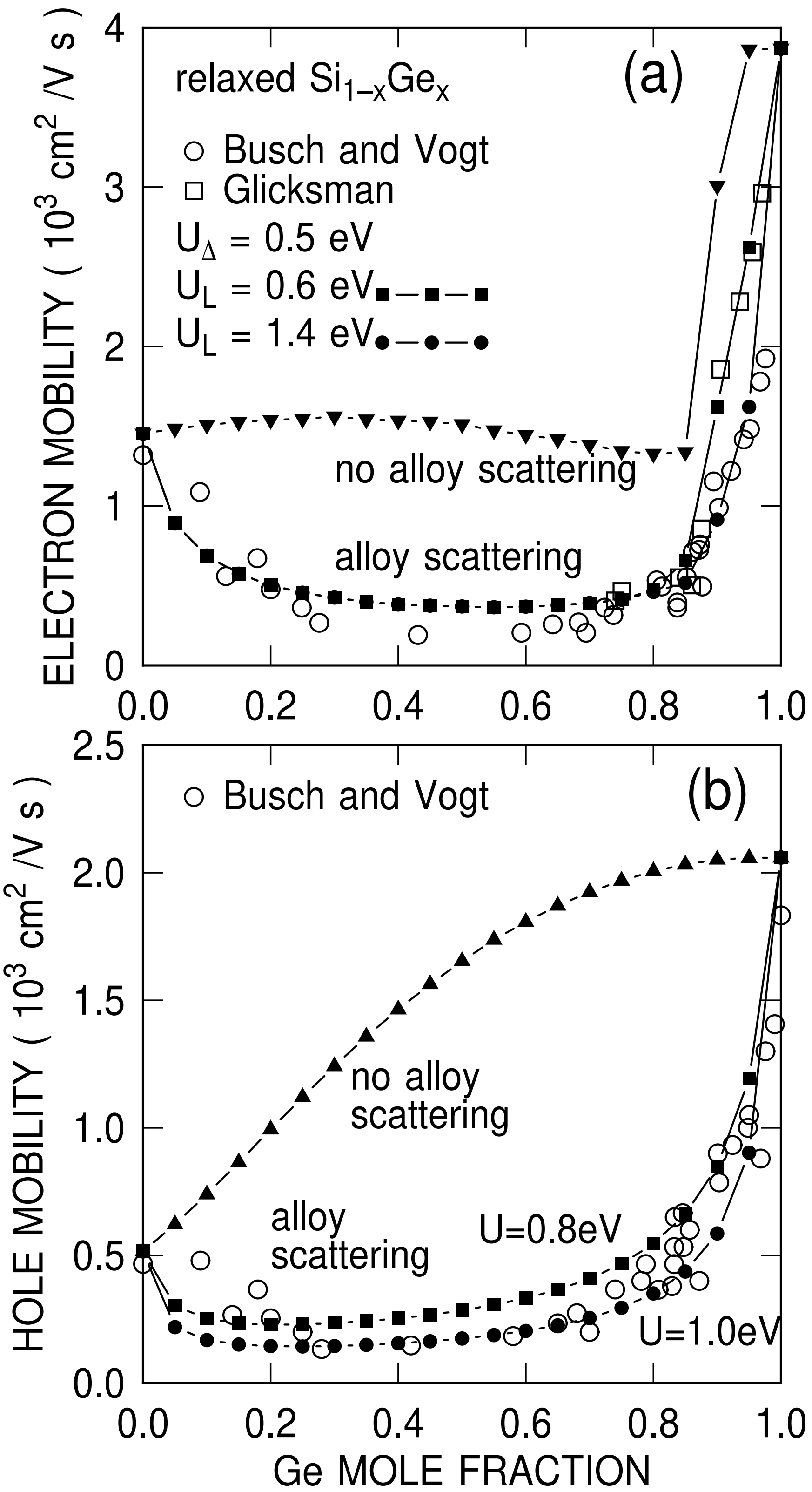

Fig. 12: Calculated phonon-limited 300 K electron (a) and hole (b) low-field mobility in relaxed $Si_{1-x}Ge_x$ alloys. The open symbols are the experimental data from Refs. 92 and 96. Results with and without the inclusion of alloy scattering are shown.

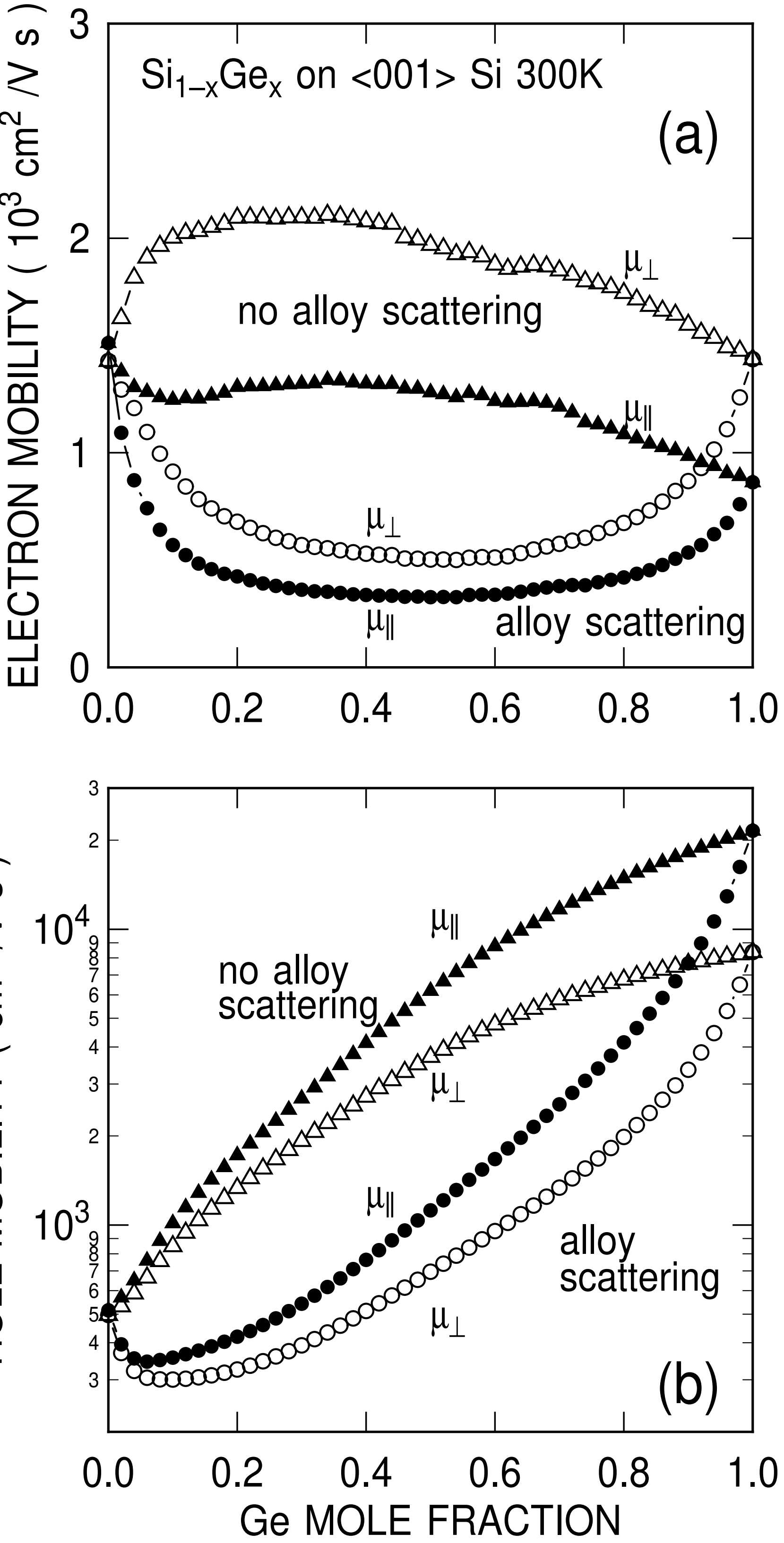

Fig. 13: Calculated phonon-limited 300 K electron (a) and hole (b) low-field mobility in $Si_{1-x}Ge_x$ alloys grown on <001> Si substrates.

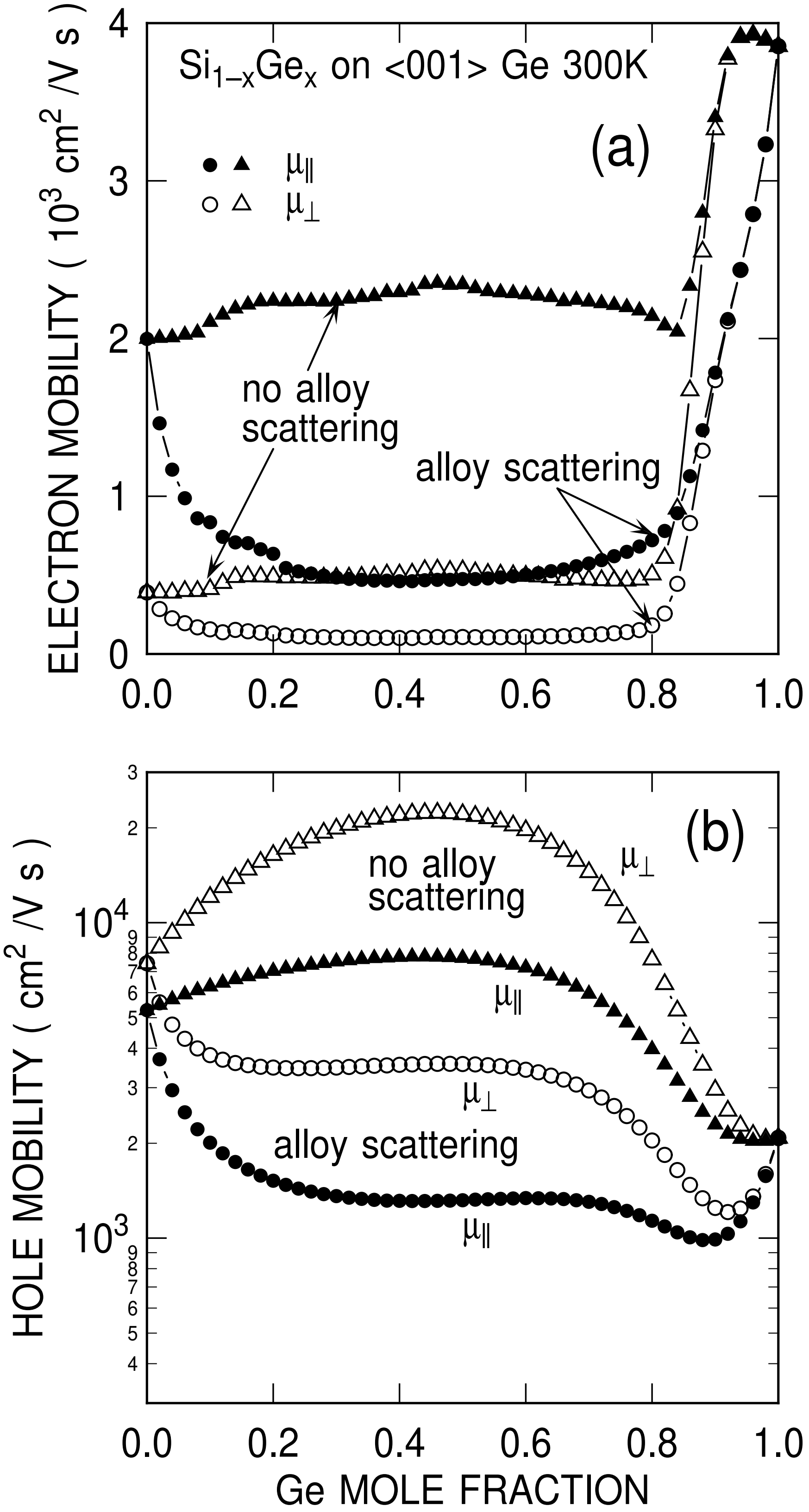

Fig. 14: Calculated phonon-limited 300 K electron (a) and hole (b) low-field mobility in $Si_{1-x}Ge_x$ alloys grown on <001> Ge substrates.